Available online at www.sciencedirect.com
ScienceDirect
Journal of Sound and Vibration 310 (2008) 313–351
JOURNAL OF SOUND AND VIBRATION
www.elsevier.com/locate/jsvi

Finite element synthesis of structural or acoustic receptances in view of practical design applications

Jean-Marie Lagache[a], Samir Assaf[b,*], Christian Schulte[b]

[a]*Architecture Mécanique Moteurs et Transmissions, PSA, Centre de la Garenne, 18, rue des Fauvelles, 92250 La Garenne Colombes, France*
[b]*Laboratoire d'Acoustique et Vibrations, Ecole Supérieure des Techniques Aéronautiques et de Construction Automobile (ESTACA), 34 rue Victor Hugo, 92300 Levallois Perret, France*

Received 29 June 2006; received in revised form 23 July 2007; accepted 30 July 2007
Available online 1 October 2007

Abstract

The present study addresses the modal synthesis of dynamic responses or receptances, which can be considered as a major issue in vibratory or acoustic design. A new method termed "method of orthocomplement" offers to increase the accuracy of modal superposition. Two apparently independent domains are considered: first, the numerical control of round-off errors in finite-dimensional models; second, the regularization of modal boundary discontinuities in infinite-dimensional formulations. Concerning the finite-dimensional systems, using the proposed method in conjunction with pseudo-inversion theorems, proves that "inertia relief corrections" remedy modal truncation problems in singular floating systems, just as static corrections do for simply supported systems. The proof is based on hitherto unpublished expressions of inertial contributions in terms of orthogonal projectors. It is worth noting that such expressions present by themselves some technical interest. Modal formulae being delivered in closed form, a thorough analysis of errors becomes possible. Special "spectrograms" are introduced to appraise the convergence of ordinary or modified modal sums. When applied to infinite-dimensional modal boundary discontinuities, the method of orthocomplement eliminates the Gibbs oscillations that affect the ordinary spectral sums, and produces the same corrected formulae as it did for finite-dimensional examples. Effective solutions for the computation of vibratory or acoustic boundary receptances, are developed in that way. The paper once again illustrates how orthogonal projectors can contribute to the determination of static corrections. Future applications to coupling problems, model reduction and modal synthesis are briefly presented at the end of the text.
© 2007 Elsevier Ltd. All rights reserved.

1. Introduction

1.1. Aims and scope

In the preliminary steps of NVH design, modification formulae such as

$$ {}^{h}\mathbf{H}_{B\leftarrow C}(\omega) = \mathbf{H}_{B\leftarrow C}(\omega) - \mathbf{H}_{B\leftarrow A}(\omega)(\mathbf{H}_{A\leftarrow A}(\omega) + \mathbf{h}(\omega))^{-1}\mathbf{H}_{A\leftarrow C}(\omega) \tag{1} $$

can be used to discuss the evolution of the transfer function from C to B , when a device of receptance **h** is inserted at A on the current structure. In this way, series of heavy computations are replaced by short matrix

*Corresponding author. Tel.: +33 1 41 27 37 18; fax: +33 1 41 27 37 42.
E-mail address: sassaf@estaca.fr (S. Assaf).

0022-460X/$ - see front matter © 2007 Elsevier Ltd. All rights reserved.
doi:10.1016/j.jsv.2007.07.051

iterations, or in the simplest cases, by analytical discussions based on complex homography and Moebius transformation [1–7].

Although the question has already been addressed in earlier references [8], the paper presents a method, termed the ''method of orthocomplement'', to control the accuracy of modal superposition during synthesis of dynamic responses or receptances, such as $\mathbf{H}_{B\leftarrow C}$, $\mathbf{H}_{B\leftarrow A}$, $\mathbf{H}_{A\leftarrow A}$, $\mathbf{H}_{A\leftarrow C}$, where A, B, C, D can be

- ***primary dofs*** as they naturally appear in the model;
- ***secondary dofs*** that are defined as linear combinations of the preceding ones, for a better understanding of structural analysis and design (least squares global rotations or translations, finite difference approximations of local strains and stresses);
- and, more generally, collections-or ***clusters***-of dofs of the preceding types.

In Section 1.2 an introduction to spectral decompositions presents what will be here called ''ordinary'', ''hybrid'' and ''accelerated'' modal series. In variance with some other papers, it is shown that modal truncation pathology in simply supported finite-dimensional frames can be remedied by static condensation [9–11]. The method of orthocomplement was initially designed to extend the preceding conclusion to more general systems showing 0 Hz singularities or ''modal boundary discontinuities'' [12,13]. The method, that takes its origin in the operations of ''static lifting'' of [14–16], is sketched out in Section 1.3. It consists in splitting up the set of algebraic or differential relations that are satisfied by the remainder in a pseudo-static sub-problem and a nested ordinary modal one. Provided additional conditions are introduced to ensure existence and uniqueness of solutions, one is led to closed-form modal representations, from which static or pseudo-static corrections can be deduced.

Section 2 of the paper relates to general finite-dimensional systems. The proposed method is first illustrated in Section 2.1 on simply supported systems. It is seen to deliver the same conclusions as before. Free finite-dimensional systems are considered in Section 2.2. Because of the 0 Hz singularity, the study has to be worked out in conjunction with three solid appendices on pseudo-inversion [17–18], denoted A, B, C at the end of the paper. The main result lies in the expression of the static ''inertia relief'' contribution as

$$(\mathbf{1}-\mathbf{\Pi}_M)(\lambda\mathbf{\Pi}+\mathbf{K})^{-1}(\mathbf{1}-\mathbf{\Pi}_M)^{\mathrm{T}}, \tag{2}$$

where ''joker'' λ is a totally arbitrary non-zero real number, and where $\mathbf{\Pi}$ and $\mathbf{\Pi}_M$ are orthogonal projectors on the nullspace, Ker($\mathbf{K}$), of the singular stiffness matrix $\mathbf{K}$ ($\mathbf{\Pi}$ for the canonical Euclidian metric, and $\mathbf{\Pi}_M$ for the metric induced by the mass matrix $\mathbf{M}$). As a practical consequence it is shown in Section 2.3 that using the inertia relief option [19] of FEM codes remedies modal truncation problems in floating frames, just as static condensation does in simply supported ones. Numerical examples are introduced in Section 2.4. It is proposed to use ''Spectrograms'', that is to say plots of cumulated modal sums, to appraise the efficiency of truncation corrections. Thereby a classification becomes possible from ''shallow'' variables based on a limited number of modes (least-squares mean displacements of structural regions), to ''deep'' variables requiring a great number of modal terms for their synthesis (isolated primary dofs or local finite differences).

Examples of extremely deep degrees of freedom are given by finite-dimensional approximations of differential problems with modal boundary discontinuities of the type considered by Kim and Kang [20]. Fig. 1, for example, relates to a two-dimensional (2D) acoustic cavity driven by a boundary loudspeaker. Diagram (a) shows the solution obtained by direct computation and diagram (b) the poor result obtained by an ordinary modal superposition. The whole difficulty lies in that rigid boundary modes are required to reconstitute a non-zero boundary velocity. Lower numerical modes, which almost exactly satisfy the set of modal equations, are not able to take the non-zero boundary condition into account. Upper modes, on the contrary, are poor numerical approximations that can develop significant boundary velocities. The modal solution thus appears as possible, but with higher-order modes than usual and at the price of numerical accuracy. Accelerated series together with static or inertia relief terms can clearly be expected to give better results than ordinary modal series.

A complete formulation is proposed in Sections 3 and 4 within the scope of infinite-dimensional differential systems. A striking feature, in that context, is that modal boundary discontinuities are associated with ''Gibbs phenomena''. As in the original discussion in 1898 by Michelson, Love, Gibbs and Poincaré, diagram

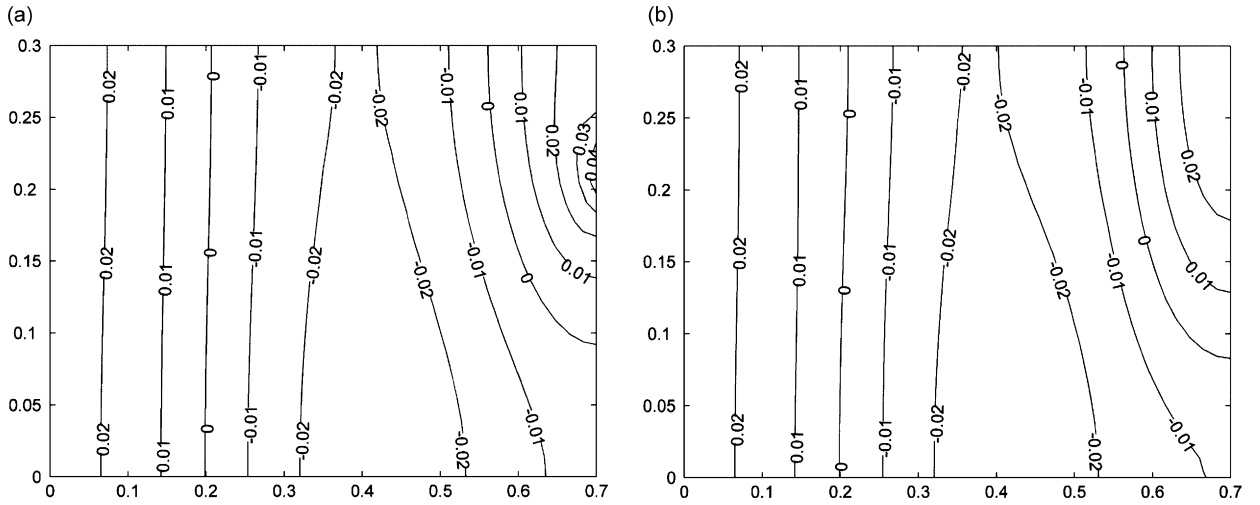

Fig. 1. Inaccurate modal rendition of the acoustic field developed at 400 Hz by a source at the boundary of a 2D cavity: (a) direct finite-element response, (b) sum of ordinary modal contributions up to 1130 Hz.

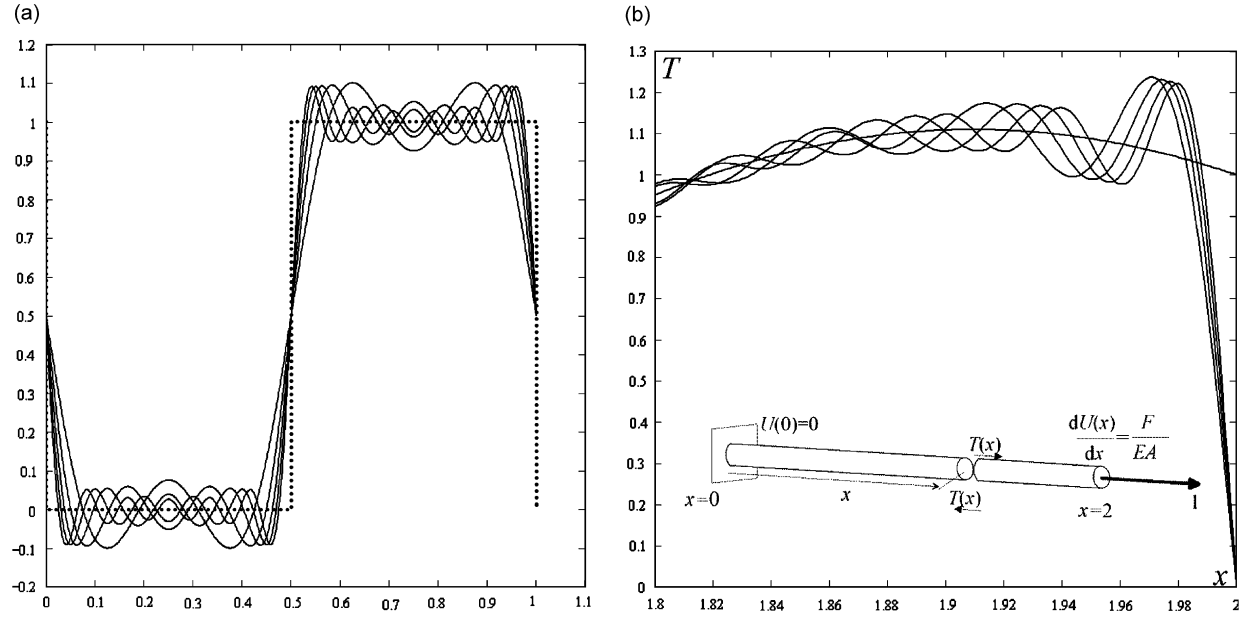

Fig. 2. Gibbs phenomenon for Fourier (a) or modal series (b).

(a) of Fig. 2 shows how ordinary partial Fourier sums can seize on a discontinuous Heaviside function, and announce the capture and resolution of the discontinuity by a familiar overshoot and ringing precisely known as the Gibbs phenomenon [12]. Diagram (b) on the same figure, relies on the fixed–free vibrating rod considered by Kim and Kang [20]. The plots, which have been drawn with a considerably reduced pace, show partial ordinary spectral sums approaching the tension at the free end of the rod. They feature the same non-decaying Gibbs oscillations as before. This is the mark that the modal series satisfies the boundary condition in a weak mathematical sense, but neither pointwise nor uniform modes of convergence can be invoked.

In Section 3, the direct computation of the theoretical orthocomplement for the problem of Kim and Kang leads to modified spectral formulae that generalize the finite-dimensional ones and eliminate the "essential"

boundary discontinuity and the related Gibbs phenomenon. "Natural" boundary conditions can be handled in a similar way, and it seemed worthwhile to illustrate this on a rod with an imposed displacement at one end and free conditions at the other.

In Section 4, the method of orthocomplement is applied to the computation of receptances at the boundary of an acoustic cavity. Interesting finite element results are obtained by using the pseudo-inverse

$$(\mathbf{1}-\mathbf{\Pi}_Q)(\lambda\mathbf{\Pi}+\mathbf{H})^{-1}, \tag{3}$$

where the acoustic finite element matrices, $\mathbf{H}$, $\mathbf{Q}$, take the place of matrices $\mathbf{K}$, $\mathbf{M}$ of Section 2. Although the main subject is receptance synthesis, a connection with more general studies on modal synthesis [21–31] is proposed in Section 5.

Because it would unnecessarily complicate the notations, damping is not explicitly taken into account. As usual in structural design, it is supposed that applicable practical formulae can be found by changing natural square frequencies ω_k^2 to their complex conventional values $\omega_k^2(1+ia)$—with a, the hysteretic proportional damping factor.

1.2. An introduction to spectral decompositions for finite simply supported systems

1.2.1. Ordinary spectral series

Let $\bar{N}$ denote the total number of dofs in a given finite vibrating system—typically up to several million in modern finite element applications. Let $\mathbf{K}$ and $\mathbf{M}$ denote the associated $\bar{N}\times\bar{N}$ positive and symmetric stiffness and mass matrix. In the simplest case when the system is simply supported, there exists at least one M-orthonormal system of $\bar{N}$ eigenmodes $\mathbf{\Psi}_m$ and $\bar{N}$ eigenfrequencies $\omega_m>0$, solution to

$$(\mathbf{K}-\mathbf{M}\omega_m^2)\mathbf{\Psi}_m=\mathbf{0}. \tag{4}$$

Those eigenmodes and eigenfrequencies allow for the synthesis of any dynamical response, according to

$$(\mathbf{K}-\mathbf{M}\omega^2)\mathbf{x}=\mathbf{f}\Leftrightarrow\mathbf{x}(\omega)=\sum_{m=1}^{\bar{N}}\frac{\mathbf{\Psi}_m\mathbf{\Psi}_m^{\mathrm{T}}}{\omega_m^2-\omega^2}\mathbf{f}. \tag{5}$$

The right hand sum will be termed as the ***ordinary modal***-or "spectral"-***series***. Although the term "series" is used here in the restricted sense of finite series, it must be noted that large values of $\bar{N}$, that are common in practical applications, require approximations by means of partial summations

$$\mathbf{x}(\omega)\simeq\sum_{m=1}^{N}\frac{\mathbf{\Psi}_m\mathbf{\Psi}_m^{\mathrm{T}}}{\omega_m^2-\omega^2}\mathbf{f} \tag{6}$$

with a number N of modes drastically smaller than $\bar{N}$.

1.2.2. Accelerated spectral series and static term

Most certainly, truncation affects modal superposition at high frequencies corresponding to the neglected modes. It should be noted, however, that the static response, $\mathbf{x}(0)$, and its truncated ordinary approximation already differ with

$$\mathbf{\varepsilon}_N(0)=\sum_{m=N+1}^{\bar{N}}\frac{\mathbf{\Psi}_m\mathbf{\Psi}_m^{\mathrm{T}}}{\omega_m^2}\mathbf{f}. \tag{7}$$

To avoid that difficulty, it has been since long proposed using the identity

$$\mathbf{x}(\omega)=\mathbf{x}(0)+[\mathbf{x}(\omega)-\mathbf{x}(0)]. \tag{8}$$

At the price of a supplementary static resolution, a class of "counter-balanced" formulae can then be derived

$$\mathbf{x}(\omega) = \mathbf{K}^{-1}\mathbf{f} + \sum_{m=1}^{\overline{N}} \left(\frac{1}{\omega_m^2 - \omega^2} - \frac{1}{\omega_m^2} \right) \boldsymbol{\Psi}_m \boldsymbol{\Psi}_m^{\mathrm{T}} \mathbf{f} \simeq \mathbf{K}^{-1}\mathbf{f} + \sum_{m=1}^{N} \left(\frac{1}{\omega_m^2 - \omega^2} - \frac{1}{\omega_m^2} \right) \boldsymbol{\Psi}_m \boldsymbol{\Psi}_m^{\mathrm{T}} \mathbf{f}. \tag{9}$$

Each modal contribution in the right member can be rearranged as

$$\frac{\omega^2}{\omega_m^2} \frac{1}{\omega_m^2 - \omega^2} \boldsymbol{\Psi}_m \boldsymbol{\Psi}_m^{\mathrm{T}} \mathbf{f}. \tag{10}$$

This only differs from the ordinary contribution in that each term is multiplied by the squared ratio of the observation frequency to the current eigenfrequency. Upper modal contributions being minimized, the series will be termed an ***accelerated modal series***.

1.2.3. Mixed spectral series and pseudo-static terms

To ensure exactness at 0 Hz without modifying the magnitudes of the contributions of lower modes, it can be proposed to fix an arbitrary integer, N, and then to split up the dynamic response in two terms

$$\begin{aligned} \mathbf{x}(\omega) &= \mathbf{x}_N(\omega) + \boldsymbol{\varepsilon}_N(\omega) \\ &= \sum_{m=1}^{N} \frac{\boldsymbol{\Psi}_m \boldsymbol{\Psi}_m^{\mathrm{T}}}{\omega_m^2 - \omega^2} \mathbf{f} + \sum_{m=N+1}^{\overline{N}} \frac{\boldsymbol{\Psi}_m \boldsymbol{\Psi}_m^{\mathrm{T}}}{\omega_m^2 - \omega^2} \mathbf{f}. \end{aligned} \tag{11}$$

The algebraic identity $\mathbf{x}(\omega) = \mathbf{x}_N(\omega) + [\mathbf{x}(0) - \mathbf{x}_N(0)] + [\boldsymbol{\varepsilon}_N(\omega) - \boldsymbol{\varepsilon}_N(0)]$ then brings

$$\mathbf{x}(\omega) = \sum_{m=1}^{N} \frac{\boldsymbol{\Psi}_m \boldsymbol{\Psi}_m^{\mathrm{T}}}{\omega_m^2 - \omega^2} \mathbf{f} + \mathbf{K}^{-1}\mathbf{f} - \sum_{m=1}^{N} \frac{\boldsymbol{\Psi}_m \boldsymbol{\Psi}_m^{\mathrm{T}}}{\omega_m^2} \mathbf{f} + \sum_{m=N+1}^{\overline{N}} \frac{\omega^2}{\omega_m^2} \frac{\boldsymbol{\Psi}_m \boldsymbol{\Psi}_m^{\mathrm{T}}}{\omega_m^2 - \omega^2} \mathbf{f} \tag{12}$$

and, since $\mathbf{K}\boldsymbol{\Psi}_m = \omega_m^2 \mathbf{M}\boldsymbol{\Psi}_m$,

$$\mathbf{x}(\omega) = \sum_{m=1}^{N} \frac{\boldsymbol{\Psi}_m \boldsymbol{\Psi}_m^{\mathrm{T}}}{\omega_m^2 - \omega^2} \mathbf{f} + \mathbf{K}^{-1} \left(\mathbf{1} - \sum_{m=1}^{N} \mathbf{M}\boldsymbol{\Psi}_m \boldsymbol{\Psi}_m^{\mathrm{T}} \right) \mathbf{f} + \sum_{m=N+1}^{\tilde{N}} \frac{\omega^2}{\omega_m^2} \frac{\boldsymbol{\Psi}_m \boldsymbol{\Psi}_m^{\mathrm{T}}}{\omega_m^2 - \omega^2} \mathbf{f}. \tag{13}$$

Formulae(12), (13) define ***mixed***—or "hybrid"-***spectral series***, the three constituents of which are an ordinary modal sum up to the order N; a pseudo-static term based on the static stiffness matrix and the first N modes; an accelerated spectral series from the order N to the maximum order $\overline{N}$. On close inspection, formulae (9) and (12) are indeed the same, save for a slight rearrangement of terms, while formulae (12) and (13) can easily be deduced one from the other by the "transmigration" of modal terms inside or outside the pseudo-static second member. The interest of mixed spectral series lies in their ability to appear in theoretical developments. Owing to the impossibility of migration of 0 Hz terms, it will be seen, however, that a minimal mixed modal formula is the ultimate solution to the singular equations that govern any floating structure.

1.2.4. Practical formulations

Hundreds of thousands of degrees of freedom are quite common in modern structural analysis. Therefore, assembling the full frequency-dependent matrix $\mathbf{H}(\omega)$ must often be viewed as a totally unfeasible task. Unlike stiffness matrices, receptances can fortunately be tailored and cut to the right dimensions without heavy condensations. Concerning the transfer from one cluster A to another cluster B, for example, the global relation $\mathbf{x} = \mathbf{H}\mathbf{f}$ reduces to $\mathbf{x}_B = \mathbf{H}_{B \leftarrow A}\mathbf{f}_A$, with $\mathbf{H}_{B \leftarrow A} = \mathbf{P}_B \mathbf{H} \mathbf{P}_A^{\mathrm{T}}$, where $\mathbf{P}_B$, $\mathbf{P}_A$ are sparse

canonical projectors:

$$P_{Ap,q} = \begin{cases} 0 & \text{if} \quad (p \neq q) \vee (q \notin A), \\ 1 & \text{if} \quad (p = q) \& (q \in A). \end{cases} \tag{14}$$

The direct computation of $\mathbf{H}_{A \leftarrow B}$ by formula (5) leads to

$$\begin{aligned} \mathbf{H}_{A \leftarrow B}(\omega) &= \mathbf{P}_A \sum_{m=1}^{\overline{N}} \frac{\boldsymbol{\Psi}_m \boldsymbol{\Psi}_m^{\mathrm{T}}}{\omega_m^2 - \omega^2} \mathbf{P}_B^{\mathrm{T}} \\ &= \sum_{m=1}^{N} \frac{(\mathbf{P}_A \boldsymbol{\Psi}_m)(\mathbf{P}_B \boldsymbol{\Psi}_m)^{\mathrm{T}}}{\omega_m^2 - \omega^2} \\ &\quad + [\![\sum_{m=N+1}^{\overline{N}} \frac{(\mathbf{P}_A \boldsymbol{\Psi}_m)(\mathbf{P}_B \boldsymbol{\Psi}_m)^{\mathrm{T}}}{\omega_m^2 - \omega^2}]\!], \end{aligned} \tag{15}$$

where the double brackets on the right contain the modal remainder for N retained modes. After the N retained eigenmodes and eigenfrequencies have been assembled in a modal matrix $\boldsymbol{\Phi} = [\boldsymbol{\Psi}_1 \boldsymbol{\Psi}_2 \cdots \boldsymbol{\Psi}_N]$, and a diagonal matrix $\boldsymbol{\Omega}$, $\Omega_{mm} = \omega_m$, it is interesting to introduce

$$\mathbf{D}(\omega) = (\Omega^2 - \omega^2 \mathbf{1})^{-1}, \tag{16}$$

thereby bringing formula (15) to the matrix form

$$\mathbf{H}_{A \leftarrow B}(\omega) \simeq \Phi_A \mathbf{D}(\omega) \Phi_B^{\mathrm{T}}, \tag{17}$$

where $\Phi_A = \mathbf{P}_A \Phi$, $\Phi_B = \mathbf{P}_B \Phi$ are reduced samples of the global modal matrix. Left-hand blocks in Fig. 3 describe as neatly as possible the overall transformation to be performed from standard modal analysis to local postprocessing. Practical limitations on storage capacities make that it is often necessary to invoke a special "set condensation" command of the finite element code, in order to provoke the preliminary sampling, $\Phi \to \Phi_\Sigma$, of the full modal matrix to the union, $\Sigma = A \cup B \cup C \cup D \cup \cdots$, of all clusters of interest.

Hybrid or simply accelerated expressions of response functions take one or another equivalent form

$$\begin{aligned} \mathbf{x}(\omega) &= \sum_{m=1}^{N} \frac{\boldsymbol{\Psi}_m \boldsymbol{\Psi}_m^{\mathrm{T}}}{\omega_m^2 - \omega^2} \mathbf{f} + \mathbf{K}^{-1} \left(\mathbf{1} - \sum_{m=1}^{N} \mathbf{M} \boldsymbol{\Psi}_m \boldsymbol{\Psi}_m^{\mathrm{T}} \right) \mathbf{f} \\ &\quad + [\![\sum_{m=N+1}^{\overline{N}} \frac{\omega^2}{\omega_m^2} \frac{\boldsymbol{\Psi}_m \boldsymbol{\Psi}_m^{\mathrm{T}}}{\omega_m^2 - \omega^2} \mathbf{f}]\!], \end{aligned} \tag{18}$$

$$\begin{aligned} \mathbf{x}(\omega) &= \sum_{m=1}^{P} \frac{\boldsymbol{\Psi}_m \boldsymbol{\Psi}_m^{\mathrm{T}}}{\omega_m^2 - \omega^2} \mathbf{f} + \mathbf{K}^{-1} \left(\mathbf{1} - \sum_{m=1}^{P} \mathbf{M} \boldsymbol{\Psi}_m \boldsymbol{\Psi}_m^{\mathrm{T}} \right) \mathbf{f} \\ &\quad + \sum_{m=P+1}^{N} \frac{\omega^2}{\omega_m^2} \frac{\boldsymbol{\Psi}_m \boldsymbol{\Psi}_m^{\mathrm{T}}}{\omega_m^2 - \omega^2} \mathbf{f} + [\![\sum_{m=N+1}^{\overline{N}} \frac{\omega^2}{\omega_m^2} \frac{\boldsymbol{\Psi}_m \boldsymbol{\Psi}_m^{\mathrm{T}}}{\omega_m^2 - \omega^2} \mathbf{f}]\!], \end{aligned} \tag{19}$$

$$\mathbf{x}(\omega) = \mathbf{K}^{-1} \ \mathbf{f} + \sum_{m=1}^{N} \frac{\omega^2}{\omega_m^2} \frac{\boldsymbol{\Psi}_m \boldsymbol{\Psi}_m^{\mathrm{T}}}{\omega_m^2 - \omega^2} \mathbf{f} + [\![\sum_{m=N+1}^{\overline{N}} \frac{\omega^2}{\omega_m^2} \frac{\boldsymbol{\Psi}_m \boldsymbol{\Psi}_m^{\mathrm{T}}}{\omega_m^2 - \omega^2} \mathbf{f}]\!]. \tag{20}$$

Owing to the non-standard pseudo-static term $\left(\mathbf{1} - \sum_{m=1}^{P} \mathbf{M} \boldsymbol{\Psi}_m \boldsymbol{\Psi}_m^{\mathrm{T}} \right) \mathbf{f}$, using mixed formulae (18), (19) is not really recommended. On the contrary, Eq. (20) brings the matrix approximation

$$\mathbf{H}_{A \leftarrow B}(\omega) \simeq \boldsymbol{\Phi}_A [\mathbf{D}(\omega) - \mathbf{D}(0)] \ \boldsymbol{\Phi}_B^{\mathrm{T}} + \mathbf{P}_A \mathbf{K}^{-1} \mathbf{P}_B^{\mathrm{T}}. \tag{21}$$

which is indeed a suitable practical formula provided the global inverse matrix, $\mathbf{K}^{-1}$, be replaced by the local compliance, $\mathbf{G}_{\Sigma \leftarrow \Sigma}$, that results from successive static resolutions.

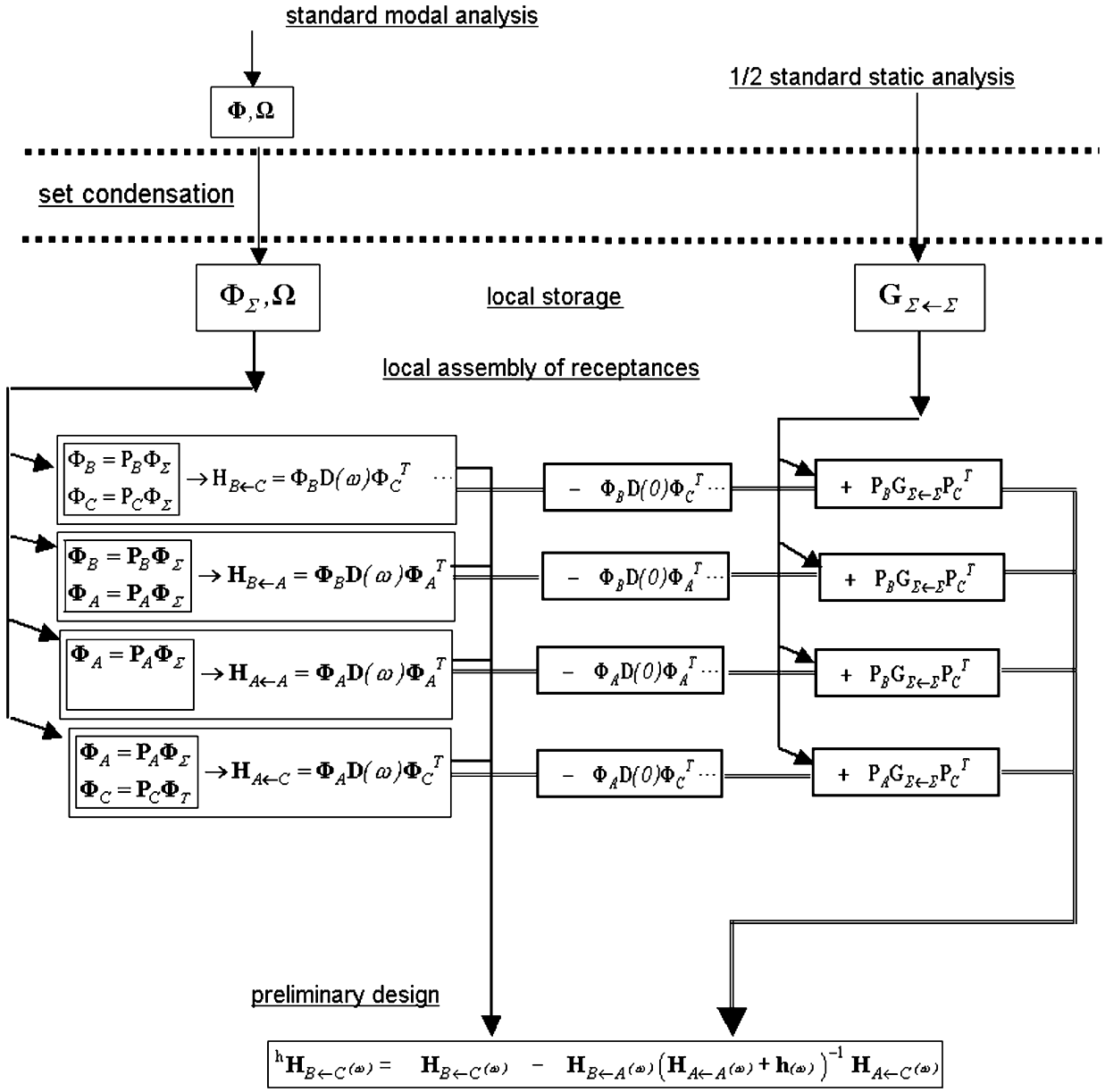

Fig. 3. Data flowchart for finite-dimensional fixed systems.

1.3. An introduction to the method of orthocomplement

The "method of orthocomplement" is an alternative method of deriving mixed modal formulae. It consists in a direct analysis of the orthocomplement $\boldsymbol{\varepsilon}_N$ in the basic projection formula

$$\mathbf{x} = \sum_{m=1}^{N} \langle \boldsymbol{\Psi}_m | x \rangle_M \boldsymbol{\Psi}_m + \boldsymbol{\varepsilon}_N = \sum_{m=1}^{N} \frac{\boldsymbol{\Psi}_m \boldsymbol{\Psi}_m^{\mathrm{T}}}{\omega_m^2 - \omega^2} \mathbf{f} + \boldsymbol{\varepsilon}_N, \tag{22}$$

where $\boldsymbol{\Psi}_m$, $m = 1,\ldots,N$, designates an M-orthonormal system of eigenmodes and $\langle .|. \rangle_M$ denotes the scalar product induced by the mass operator $\mathbf{M}$.

The analysis proceeds in three steps:

(a) *Forward step*—The set of equations that characterizes $\boldsymbol{\varepsilon}_N$ is split into two nested sub-problems, in such a way that $\boldsymbol{\varepsilon}_N$ is written as $\boldsymbol{\varepsilon}_N = \boldsymbol{\eta}_N + \boldsymbol{\rho}_N$, where
- $\boldsymbol{\eta}_N$ is the solution to a pseudo-static problem (A), with the only static operator in the first member;
- $\boldsymbol{\rho}_N$ is the solution to a dynamical problem (B), with the full dynamical operator in the first member and the pseudo-static solution $\boldsymbol{\eta}_N$ in the second member.

The consistency of the decomposition rests on the solvability of problem (A). Checking that point is thus the major technical task at the considered stage.

(b) *Coordination step*—Once a solution to problem (A) is found, rather than assembling problem (B) to compute $\boldsymbol{\rho}_N$, it is suggested to proceed as follows:
- in case the static operator is not singular, the modal projections of $\boldsymbol{\rho}_N$ can be expressed in terms of the corresponding projections of $\boldsymbol{\eta}_N$: $\langle \boldsymbol{\Psi}_k | \boldsymbol{\rho}_N \rangle = f\langle \boldsymbol{\Psi}_k | \boldsymbol{\eta}_N \rangle$. Surprisingly the projections $\langle \boldsymbol{\Psi}_k | \boldsymbol{\eta}_N \rangle$ are directly computable, and the modal projections of $\boldsymbol{\rho}_N$ can then be found by composition of the two preceding sets of formulae.
- in case the static operator is singular, and the solvability conditions are fulfilled, solution $\boldsymbol{\eta}_N$ is not unique and both problems (A) and (B) suffer from indetermination. Normal elastic modes at positive frequencies can bear the same treatment as before, but the σ rigid modes at 0 Hz would provoke divisions by zero. A set of complementary relations $\langle \boldsymbol{\Psi}_k | \boldsymbol{\eta}_N \rangle = 0$, $k = 1, \ldots, \sigma$ can then be added to problem (A), that renders its solution $\boldsymbol{\eta}_N$ unique, and annihilates the corresponding projections $\langle \boldsymbol{\Psi}_k | \boldsymbol{\rho}_N \rangle = f(\langle \boldsymbol{\Psi}_k | \boldsymbol{\eta}_N \rangle)$, $k = 1, \ldots, \sigma$. All other projections being known, a complete solution becomes possible.

(c) *Backward step*—The solution is finally obtained by assembling the ordinary modal sum, the solution to the pseudo-static problem and the spectral development of $\boldsymbol{\rho}_N$. It must be noted that the last term will appear as an accelerated modal series in all the following examples.

2. Study of general finite systems by the method of orthocomplement

2.1. The simple case of fixed finite systems

A first application of the method can now be performed on fixed finite systems, with non-singular stiffness matrices $\mathbf{K}$. The results have already been derived in Section 1.2. The development is just intended to illustrate the general methodology, and to provide guidelines to study more complicated singular systems.

(a) *Forward step*: As a consequence of the equations of motion, the orthocomplement is seen to satisfy

$$(\mathbf{K} - \mathbf{M}\omega^2)\boldsymbol{\varepsilon}_N = \mathbf{f} - \sum_{m=1}^{N} (\mathbf{K} - \mathbf{M}\omega^2) \frac{\boldsymbol{\Psi}_m \boldsymbol{\Psi}_m^{\mathrm{T}} \mathbf{f}}{\omega_m^2 - \omega^2} = \mathbf{f} - \sum_{m=1}^{N} \mathbf{M}(\omega_m^2 - \omega^2) \frac{\boldsymbol{\Psi}_m \boldsymbol{\Psi}_m^{\mathrm{T}} \mathbf{f}}{\omega_m^2 - \omega^2}. \tag{23}$$

This last problem can be split up into two nested sub-problems, A, B, according to the following scheme:

$$(\mathbf{K} - \mathbf{M}\omega^2)\boldsymbol{\varepsilon}_N = \left(1 - \sum_{m=1}^{N} \mathbf{M}\boldsymbol{\Psi}_m \boldsymbol{\Psi}_m^{\mathrm{T}}\right)\mathbf{f} \Leftrightarrow \boldsymbol{\varepsilon}_N = \boldsymbol{\eta}_N + \boldsymbol{\rho}_N \left\langle \begin{array}{ll} \mathbf{K}\boldsymbol{\eta}_N = \left(1 - \sum_{m=1}^{N} \mathbf{M}\boldsymbol{\Psi}_m \boldsymbol{\Psi}_m^{\mathrm{T}}\right)\mathbf{f} & (A) \\ (\mathbf{K} - \mathbf{M}\omega^2)\boldsymbol{\rho}_N = \mathbf{M}\omega^2 \boldsymbol{\eta}_N & (B) \end{array} \right. . \tag{24}$$

Since $\det \mathbf{K} \neq 0$, the decomposition is coherent and both sub-problems have a unique solution.

(b) *Coordination step*: Problem (B) is a classical dynamical problem whose solution has the spectral representation

$$\boldsymbol{\rho}_N = \sum_{m=1}^{\overline{N}} \frac{\omega^2}{\omega_m^2 - \omega^2} \boldsymbol{\Psi}_m \boldsymbol{\Psi}_m^{\mathrm{T}} \mathbf{M} \boldsymbol{\eta}_N. \tag{25}$$

The M-projections on the kth eigenmode of $\boldsymbol{\rho}_N$ and $\boldsymbol{\eta}_N$ are linked by

$$\boldsymbol{\Psi}_k^{\mathrm{T}}\mathbf{M}\boldsymbol{\rho}_N = \sum_{m=1}^{\overline{N}} \frac{\boldsymbol{\Psi}_k^{\mathrm{T}}\mathbf{M}\boldsymbol{\Psi}_m\boldsymbol{\Psi}_m^{\mathrm{T}}\mathbf{M}\omega^2\boldsymbol{\eta}_N}{\omega_m^2-\omega^2} = \sum_{m=1}^{\overline{N}} \frac{\omega^2}{\omega_m^2-\omega^2}\underbrace{\boldsymbol{\Psi}_k^{\mathrm{T}}\mathbf{M}\boldsymbol{\Psi}_m}_{\delta_{km}}\boldsymbol{\Psi}_m^{\mathrm{T}}\mathbf{M}\boldsymbol{\eta}_N = \frac{\omega^2}{\omega_k^2-\omega^2}\boldsymbol{\Psi}_k^{\mathrm{T}}\mathbf{M}\boldsymbol{\eta}_N \tag{26}$$

where the transient δ_{km} denotes the Kronecker symbol.

According to Eq. (24), the solution to problem (A) writes

$$\boldsymbol{\eta}_N = \mathbf{K}^{-1}\left(1-\sum_{m=1}^{N}\mathbf{M}\boldsymbol{\Psi}_m\boldsymbol{\Psi}_m^{\mathrm{T}}\right)\mathbf{f} \tag{27}$$

and it should be possible to compute modal projections $\boldsymbol{\Psi}_k^{\mathrm{T}}\mathbf{M}\boldsymbol{\eta}_N$ by using the modal identities $\boldsymbol{\Psi}_k^{\mathrm{T}}\mathbf{M} = (1/\omega_k^2)\boldsymbol{\Psi}_k^{\mathrm{T}}\mathbf{K}$; as a matter of fact, this brings

$$\begin{aligned}\boldsymbol{\Psi}_k^{\mathrm{T}}\mathbf{M}\boldsymbol{\eta}_N &= \boldsymbol{\Psi}_k^{\mathrm{T}}\mathbf{M}\mathbf{K}^{-1}\mathbf{f} - \sum_{m=1}^{N}\boldsymbol{\Psi}_k^{\mathrm{T}}\mathbf{M}\mathbf{K}^{-1}\mathbf{M}\boldsymbol{\Psi}_m\boldsymbol{\Psi}_m^{\mathrm{T}}\mathbf{f} = \frac{1}{\omega_k^2}\underbrace{\boldsymbol{\Psi}_k^{\mathrm{T}}\mathbf{K}\mathbf{K}^{-1}}_{\boldsymbol{\Psi}_k^{\mathrm{T}}}\mathbf{f} - \frac{1}{\omega_k^2}\sum_{m=1}^{N}\underbrace{\boldsymbol{\Psi}_k^{\mathrm{T}}\mathbf{K}\mathbf{K}^{-1}}_{\boldsymbol{\Psi}_k^{\mathrm{T}}}\mathbf{M}\boldsymbol{\Psi}_m\boldsymbol{\Psi}_m^{\mathrm{T}}\mathbf{f}\\ &= \ldots = \frac{1}{\omega_k^2}\boldsymbol{\Psi}_k^{\mathrm{T}}\mathbf{f} - \frac{1}{\omega_k^2}\sum_{m\leqslant N}\underbrace{\boldsymbol{\Psi}_k^{\mathrm{T}}\mathbf{M}\boldsymbol{\Psi}_m}_{\delta_{km}}\boldsymbol{\Psi}_m^{\mathrm{T}}\mathbf{f} = \begin{cases} 0 & \text{if} \quad 1\leqslant k\leqslant N,\\ \dfrac{1}{\omega_k^2}\boldsymbol{\Psi}_k^{\mathrm{T}}\mathbf{f} & \text{if} \quad k>N.\end{cases}\end{aligned} \tag{28}$$

By composition of the two preceding sets of formulae, the M-projections of $\boldsymbol{\rho}_N$ are given by

$$\boldsymbol{\Psi}_k^{\mathrm{T}}\mathbf{M}\boldsymbol{\rho}_N = \frac{\omega^2}{\omega_k^2-\omega^2}\boldsymbol{\Psi}_k^{\mathrm{T}}\mathbf{M}\boldsymbol{\eta}_N = \begin{cases} 0 & \text{if} \quad k\leqslant N,\\ \dfrac{\omega^2}{\omega_k^2}\dfrac{1}{\omega_k^2-\omega^2}\boldsymbol{\Psi}_k^{\mathrm{T}}\mathbf{f} & \text{if} \quad k>N.\end{cases} \tag{29}$$

(c) *Backward step*: Assembling the solutions to problems (A), (B) and the ordinary modal sum up to order N then brings the result of Section 1.2 again

$$\mathbf{x} = \sum_{k=1}^{N}\frac{\boldsymbol{\Psi}_k\boldsymbol{\Psi}_k^{\mathrm{T}}}{\omega_k^2-\omega^2}\mathbf{f} + \mathbf{K}^{-1}\left(\mathbf{f}-\sum_{m=1}^{N}\mathbf{M}\boldsymbol{\Psi}_m\boldsymbol{\Psi}_m^{\mathrm{T}}\mathbf{f}\right) + \sum_{k=N+1}^{\overline{N}}\frac{\omega^2}{\omega_k^2}\frac{\boldsymbol{\Psi}_k\boldsymbol{\Psi}_k^{\mathrm{T}}}{\omega_k^2-\omega^2}\mathbf{f}. \tag{30}$$

2.2. Floating finite systems

The case when $\det\mathbf{K} = 0$ is now considered.

(a) *Forward step*: This is the same computation as before, with the slight difference, that σ rigid modes $-\sigma = 1$, 3 or 6—must now be carefully distinguished:

$$\boldsymbol{\varepsilon}_N = \boldsymbol{\eta}_N + \boldsymbol{\rho}_N\left\langle \begin{array}{c}\mathbf{K}\boldsymbol{\eta}_N = \left(1-\sum_{m=1}^{\sigma}\mathbf{M}\boldsymbol{\Psi}_m\boldsymbol{\Psi}_m^{\mathrm{T}} - \sum_{m=\sigma+1}^{N}\mathbf{M}\boldsymbol{\Psi}_m\boldsymbol{\Psi}_m^{\mathrm{T}}\right)\mathbf{f} \quad \text{(A)}\\ (\mathbf{K}-\mathbf{M}\omega^2)\boldsymbol{\rho}_N = \mathbf{M}\omega^2\boldsymbol{\eta}_N \quad \text{(B)}\end{array}\right. \tag{31}$$

Although $\det\mathbf{K} = 0$, problem (A) is soluble. As a matter of fact, equation (A) imposes on operator $\mathbf{K}$ to map solution $\boldsymbol{\eta}_N$ to $\varphi = \mathbf{f} - \sum_{m=1}^{N}\mathbf{M}\boldsymbol{\Psi}_m^{\mathrm{T}}\boldsymbol{\Psi}_m\mathbf{f}$. The problem is therefore soluble iff $\varphi\in\mathrm{Im}(\mathbf{K})$ or, according to Lagrange's lemma of Appendix A, iff $\varphi\perp\mathrm{Ker}(\mathbf{K})$. The σ independent rigid modes, $\boldsymbol{\Psi}_k$, $k = 1,\ldots,\sigma$, give precisely:

$$\boldsymbol{\Psi}_k^{\mathrm{T}}\varphi = \boldsymbol{\Psi}_k^{\mathrm{T}}\mathbf{f} - \sum_{m=1}^{N}\boldsymbol{\Psi}_k^{\mathrm{T}}\mathbf{M}\boldsymbol{\Psi}_m\boldsymbol{\Psi}_k^{\mathrm{T}}\mathbf{f} = \boldsymbol{\Psi}_k^{\mathrm{T}}\mathbf{f} - \sum_{m=1}^{N}\delta_{km}\boldsymbol{\Psi}_k^{\mathrm{T}}\mathbf{f} = \boldsymbol{\Psi}_k^{\mathrm{T}}\mathbf{f} - \boldsymbol{\Psi}_k^{\mathrm{T}}\mathbf{f} = 0, \tag{32}$$

which shows the last orthogonality condition to be fulfilled.

(b) *Coordination step*: Problem (B) is a classical dynamical problem whose solution has the spectral representation

$$\boldsymbol{\rho}_N = -\sum_{m=1}^{\sigma} \boldsymbol{\Psi}_m \boldsymbol{\Psi}_m^{\mathrm{T}} \mathbf{M} \boldsymbol{\eta}_N + \sum_{m=\sigma+1}^{\overline{N}} \frac{\omega^2}{\omega_m^2 - \omega^2} \boldsymbol{\Psi}_m \boldsymbol{\Psi}_m^{\mathrm{T}} \mathbf{M} \boldsymbol{\eta}_N. \tag{33}$$

The M-projections of $\boldsymbol{\rho}_N$ and $\boldsymbol{\eta}_N$ are therefore linked by

$$\boldsymbol{\Psi}_k^{\mathrm{T}} \mathbf{M} \boldsymbol{\rho}_N = \frac{\omega^2}{\omega_k^2 - \omega^2} \boldsymbol{\Psi}_k^{\mathrm{T}} \mathbf{M} \boldsymbol{\eta}_N \tag{34}$$

with the especially important relations $\boldsymbol{\Psi}_k^{\mathrm{T}} \mathbf{M} \boldsymbol{\rho}_N = -\boldsymbol{\Psi}_k^{\mathrm{T}} \mathbf{M} \boldsymbol{\eta}_N$, $k = 1, \ldots, \sigma$.

In contrast to the regular case, modal projections $\boldsymbol{\Psi}_k^{\mathrm{T}} \mathbf{M} \boldsymbol{\eta}_N$ cannot be easily computed since:

- matrix $\mathbf{K}$ has no inverse and expression (27) of $\boldsymbol{\eta}_N$ must be replaced by an adequate pseudo-inverse equivalent;
- the elimination condition that was used in Eq. (28), $\boldsymbol{\Psi}_k^{\mathrm{T}} \mathbf{M} = \omega_k^{-2} \boldsymbol{\Psi}_k^{\mathrm{T}} \mathbf{K}$, only works when $\omega_k \neq 0$, but not when $\boldsymbol{\Psi}_k$ is one or the other of the σ rigid modes.

It is now of some importance to remark that matrix $\mathbf{K}$ being of rank $\overline{N} - \sigma$, problem (A) needs σ additional independent relations for its solution to be determined. At the same time, such a set of σ relations corresponds to what should be added to the set of known projections of $\boldsymbol{\eta}_N$ to definitely fix the solution to problem (B).

A quite natural choice of additional conditions is

$$\boldsymbol{\Psi}_k^{\mathrm{T}} \mathbf{M} \boldsymbol{\eta}_N = 0, \quad 1 \leqslant k \leqslant \sigma. \tag{35}$$

Problem (A) can then be reformulated as

$$\left.\begin{aligned} \mathbf{K} \boldsymbol{\eta}_N &= \left(1 - \sum_{m=1}^{\sigma} \mathbf{M} \boldsymbol{\Psi}_m \boldsymbol{\Psi}_m^{\mathrm{T}} - \sum_{m=\sigma+1}^{N} \mathbf{M} \boldsymbol{\Psi}_m \boldsymbol{\Psi}_m^{\mathrm{T}}\right) \mathbf{f} \\ \boldsymbol{\Psi}_k^{\mathrm{T}} \mathbf{M} \boldsymbol{\eta}_N &= 0, \quad k = 1, \ldots \sigma \end{aligned}\right\}. \tag{36}$$

Owing to the fact that rigid modes $\boldsymbol{\Psi}_k$, $1 \leqslant k \leqslant \sigma$, form a basis of the nullspace of $\mathbf{K}$, Eq. (36) define a unique solution

$$\boldsymbol{\eta}_N = \mathbf{K}^{\dagger[M]} \left(\mathbf{1} - \sum_{m=1}^{\sigma} \mathbf{M} \boldsymbol{\Psi}_m \boldsymbol{\Psi}_m^{\mathrm{T}} - \sum_{m=\sigma+1}^{N} \mathbf{M} \boldsymbol{\Psi}_m \boldsymbol{\Psi}_m^{\mathrm{T}}\right) \mathbf{f} \tag{37}$$

in terms of the pseudo-inverse $\mathbf{K}^{\dagger[M]}$ of Appendix B. Using the complete mathematical expression developed in Appendix B yields

$$\boldsymbol{\eta}_N = (\mathbf{1} - \boldsymbol{\Pi}_M)(\lambda \boldsymbol{\Pi} + \mathbf{K})^{-1} \left(1 - \sum_{m=1}^{\sigma} \mathbf{M} \boldsymbol{\Psi}_m \boldsymbol{\Psi}_m^{\mathrm{T}} - \sum_{m=\sigma+1}^{N} \mathbf{M} \boldsymbol{\Psi}_m \boldsymbol{\Psi}_m^{\mathrm{T}}\right) \mathbf{f}, \tag{38}$$

where λ is an arbitrary non-zero number, and $\boldsymbol{\Pi}_M$, $\boldsymbol{\Pi}$ denote the orthogonal projectors on the set of all rigid modes, respectively, for the M-metric and for the canonical Euclidian one.

The σ first modal projections of $\boldsymbol{\rho}_N$ are zero, since Eqs. (34) and (35) yield

$$\boldsymbol{\Psi}_k^{\mathrm{T}} \mathbf{M} \boldsymbol{\rho}_N = -\boldsymbol{\Psi}_k^{\mathrm{T}} \ \mathbf{M} \boldsymbol{\eta}_N = 0, \quad k = 1, \ldots, \sigma. \tag{39}$$

To prepare for the computation of other projections, it can be remarked that, for any index $k > \sigma$, $\mathbf{x} = \mathbf{K}^{\dagger[M]} \mathbf{K} \boldsymbol{\Psi}_k$ is the only solution to $\mathbf{K}\mathbf{x} = \mathbf{K}\boldsymbol{\Psi}_k$ that satisfies $\boldsymbol{\Psi}_p^{\mathrm{T}} \mathbf{M} \mathbf{x} = 0$, $1 \leqslant p \leqslant \sigma$. But, since $\boldsymbol{\Psi}_k$ itself trivially satisfies the above algebraic equation and orthogonality conditions, it is possible to write $\mathbf{x} = \boldsymbol{\Psi}_k$ and therefore use the relation

$$\mathbf{K}^{\dagger[M]} \mathbf{K} \boldsymbol{\Psi}_k = \boldsymbol{\Psi}_k \quad \text{for any index } k > \sigma \tag{40}$$

in place of the relation $\mathbf{K}^{-1}\mathbf{K} = 1$ of the regular case.

As a consequence, for any $k>\sigma$, the kth M-projection of $\boldsymbol{\eta}_N$ can be computed as follows:

$$\boldsymbol{\Psi}_k^{\mathrm{T}}\mathbf{M}\boldsymbol{\eta}_N = \boldsymbol{\Psi}_k^{\mathrm{T}}\mathbf{M}\mathbf{K}^{\dagger[M]}\mathbf{f} - \sum_{m=1}^{N}\boldsymbol{\Psi}_k^{\mathrm{T}}\mathbf{M}\mathbf{K}^{\dagger[M]}\mathbf{M}\boldsymbol{\Psi}_m\boldsymbol{\Psi}_m^{\mathrm{T}}\mathbf{f} = \frac{1}{\omega_k^2}\underbrace{\boldsymbol{\Psi}_m^{\mathrm{T}}\mathbf{K}\mathbf{K}^{\dagger[M]}}_{\boldsymbol{\Psi}_k^{\mathrm{T}}}\mathbf{f} - \frac{1}{\omega_k^2}\sum_{m=1}^{N}\underbrace{\boldsymbol{\Psi}_k^{\mathrm{T}}\mathbf{K}\mathbf{K}^{\dagger[M]}}_{\boldsymbol{\Psi}_k^{\mathrm{T}}}\mathbf{M}\boldsymbol{\Psi}_m\boldsymbol{\Psi}_m^{\mathrm{T}}\mathbf{f}$$

$$= \cdots = \frac{1}{\omega_k^2}\boldsymbol{\Psi}_k^{\mathrm{T}}\mathbf{f} - \frac{1}{\omega_k^2}\sum_{m=1}^{N}\underbrace{\boldsymbol{\Psi}_k^{\mathrm{T}}\mathbf{M}\boldsymbol{\Psi}_m}_{\delta_{km}}\boldsymbol{\Psi}_m^{\mathrm{T}}\mathbf{f} = \begin{cases} 0 & \text{if} \quad \sigma+1\leqslant k\leqslant N, \\ \dfrac{1}{\omega_k^2}\boldsymbol{\Psi}_k^{\mathrm{T}}\mathbf{f} & \text{if} \quad k>N. \end{cases}$$

From Eqs. (34), (35), the modal projections of $\boldsymbol{\rho}_N$ are given by

$$\boldsymbol{\Psi}_k^{\mathrm{T}}\mathbf{M}\boldsymbol{\rho}_N = \begin{cases} 0 & \text{if} \quad 1\leqslant k\leqslant N, \\ \dfrac{\omega^2}{\omega_k^2}\dfrac{1}{\omega_k^2-\omega^2}\boldsymbol{\Psi}_k^{\mathrm{T}}\mathbf{f} & \text{if} \quad k>N. \end{cases} \tag{41}$$

(c) *Backward step*: It results from Eq. (41), that the solution to problem (B), $\boldsymbol{\rho}_N$, appears as an accelerated series, with the same expression as in the regular case of Section 2.1. The same thing can be said of the pseudo-static term, except that the inverse $\mathbf{K}^{-1}$ is replaced by the pseudo-inverse $\mathbf{K}^{\dagger[M]}$. As a conclusion, the complete dynamical response can be given as

$$\mathbf{x} = \sum_{k=1}^{N}\frac{\boldsymbol{\Psi}_k\boldsymbol{\Psi}_k^{\mathrm{T}}}{\omega_k^2-\omega^2}\mathbf{f} + K^{\dagger[M]}\left(\mathbf{f} - \sum_{m=1}^{N}\mathbf{M}\boldsymbol{\Psi}_m\boldsymbol{\Psi}_m^{\mathrm{T}}\mathbf{f}\right) + \sum_{k=N+1}^{\overline{N}}\frac{\omega^2}{\omega_k^2}\frac{\boldsymbol{\Psi}_k\boldsymbol{\Psi}_k^{\mathrm{T}}}{\omega_k^2-\omega^2}\mathbf{f}, \tag{42}$$

where the pseudo-inverse $\mathbf{K}^{\dagger[M]}$ is defined by Eq. (36).

2.3. Practical computation: inertia relief

After truncation formula (42) gives

$$\mathbf{x} \simeq \sum_{m=1}^{N}\frac{\boldsymbol{\Psi}_m\boldsymbol{\Psi}_m^{\mathrm{T}}}{\omega_m^2-\omega^2}\mathbf{f} + \mathbf{K}^{\dagger[M]}\left(\mathbf{f} - \sum_{m=1}^{\sigma}\mathbf{M}\boldsymbol{\Psi}_m\boldsymbol{\Psi}_m^{\mathrm{T}}\mathbf{f} - \sum_{m=\sigma+1}^{N}\mathbf{M}\boldsymbol{\Psi}_m\boldsymbol{\Psi}_m^{\mathrm{T}}\,\mathbf{f}\right). \tag{43}$$

Just as in the regular case, the problem lies in the non-standard assembling of the pseudo-static second member problem. A good remedy was found earlier to consist in the ''transmigration'' of modal terms outside the right-hand parentheses. This perfectly works for modal contributions at strictly positive frequencies, since by (40), it is possible to write

$$\mathbf{K}^{\dagger[M]}\left(\sum_{m=\sigma+1}^{N}\mathbf{M}\boldsymbol{\Psi}_m\boldsymbol{\Psi}_m^{\mathrm{T}}\mathbf{f}\right) = \sum_{m=\sigma+1}^{N}\frac{1}{\omega_m^2}\mathbf{K}^{\dagger[M]}\mathbf{K}\boldsymbol{\Psi}_m\boldsymbol{\Psi}_m^{\mathrm{T}}\mathbf{f} = \sum_{m=\sigma+1}^{N}\frac{1}{\omega_m^2}\boldsymbol{\Psi}_m\boldsymbol{\Psi}_m^{\mathrm{T}}\mathbf{f}. \tag{44}$$

The rule being not valid for the σ rigid modes at 0 frequencies, it should be clear that

$$\mathbf{x} \simeq \sum_{m=1}^{N}\frac{1}{\omega_m^2-\omega^2}\boldsymbol{\Psi}_m\boldsymbol{\Psi}_m^{\mathrm{T}}\mathbf{f} - \sum_{m=\sigma+1}^{N}\frac{1}{\omega_m^2}\boldsymbol{\Psi}_m\boldsymbol{\Psi}_m^{\mathrm{T}}\mathbf{f} + \mathbf{K}^{\dagger[M]}\left(1 - \sum_{m=1}^{\sigma}\mathbf{M}\boldsymbol{\Psi}_m\boldsymbol{\Psi}_m^{\mathrm{T}}\right)\mathbf{f}, \tag{45}$$

is the best that can be done.

A slight rearrangement of terms then yields

$$\mathbf{x} \simeq \frac{-1}{\omega^2}\sum_{m=1}^{\sigma}\boldsymbol{\Psi}_m\boldsymbol{\Psi}_m^{\mathrm{T}}\mathbf{f} + \sum_{m=\sigma+1}^{N}\frac{\omega^2}{\omega_m^2}\frac{1}{\omega_m^2-\omega^2}\boldsymbol{\Psi}_m\boldsymbol{\Psi}_m^{\mathrm{T}}\mathbf{f} + \mathbf{K}^{\dagger[M]}\left(\mathbf{1} - \sum_{m=1}^{\sigma}\mathbf{M}\boldsymbol{\Psi}_m\boldsymbol{\Psi}_m^{\mathrm{T}}\right)\mathbf{f} \tag{46}$$

from which it becomes possible to state that the dynamic response $\mathbf{x}$ of any singular floating system can be approached by the superposition of

- an ordinary modal sum for the σ rigid modes;
- an accelerated sum for "elastic" modes of orders greater than σ; and
- a pseudo-static term based on the σ rigid modes.

It should be noted that Eq. (42), before truncation, gives the remainder as an accelerated series.

The pseudo-static term remains to be interpreted. For the sake of readability, mathematical theorems on pseudo-inversion have been gathered in three appendices—labelled A, B, C—at the end of the text. Appendix C addresses the Laurent expansion at 0 Hz of the dynamic response in a singular floating system. It contains the following interpretation of the pseudo-static term:

$$\mathbf{K}^{\dagger[M]}\left(1-\sum_{m=1}^{\sigma}\mathbf{M}\boldsymbol{\Psi}_m\boldsymbol{\Psi}_m^{\mathrm{T}}\right)\mathbf{f}=\begin{Bmatrix}\text{coefficient of } \omega^0 \text{ in the Laurent expansion of } \mathbf{x}\\ \text{inertia relief response at 0 Hz}\\ (\mathbf{1}-\boldsymbol{\Pi}_M)(\lambda\boldsymbol{\Pi}+\mathbf{K})^{-1}(\mathbf{1}-\boldsymbol{\Pi}_M)^{\mathrm{T}}\mathbf{f}\end{Bmatrix}. \tag{47}$$

As already mentioned in presenting formula (38), λ is an arbitrary non-zero number, and $\boldsymbol{\Pi}$, $\boldsymbol{\Pi}_M$, are orthogonal projectors onto the vector set of rigid motions, respectively, for the canonical Euclidian metric and that induced by the mass matrix $\mathbf{M}$.

Although there is no difficulty in evaluating the ordinary modal sum at 0 Hz, another interesting result is that

$$\sum_{m=1}^{\sigma}\boldsymbol{\Psi}_m\boldsymbol{\Psi}_m^{\mathrm{T}}\mathbf{f}=\begin{Bmatrix}\text{coefficient of } \omega^{-2} \text{ in the Laurent expansion of } \mathbf{x}\\ \text{rigid body acceleration field at 0 Hz}\\ \boldsymbol{\Pi}_M^{\mathrm{T}}\mathbf{f}=\mathbf{S}(\mathbf{S}^{\mathrm{T}}\mathbf{M}\mathbf{S})^{-1}\mathbf{S}^{\mathrm{T}}\mathbf{f}\end{Bmatrix} \tag{48}$$

with $\mathbf{S}$, the matrix whose columns span the set of rigid motions.

For the purpose of computing the transfer matrix from a cluster A to a cluster B, formulae (45) or (46) can be rewritten as

$$\mathbf{H}_{A\leftarrow B}(\omega)\simeq\boldsymbol{\Phi}_A\mathbf{D}(\omega)\boldsymbol{\Phi}_B^{\mathrm{T}}-\boldsymbol{\Phi}_A\mathbf{D}^{\oplus}(0)\boldsymbol{\Phi}_B^{\mathrm{T}}+\mathbf{P}_A(\mathbf{1}-\boldsymbol{\Pi}_M)(\lambda\boldsymbol{\Pi}+\mathbf{K})^{-1}(\mathbf{1}-\boldsymbol{\Pi}_M)^{\mathrm{T}}\mathbf{P}_B^{\mathrm{T}}, \tag{49}$$

which is the exact counterpart of formula (21) for fixed systems. The notation $\mathbf{D}(\omega)$ still refers to the diagonal $D_{mm}=(\omega_m^2-\omega^2)^{-1}$, while $\mathbf{D}^{\oplus}$ is the restriction of the preceding to non-zero eigenfrequencies:

$$\mathbf{D}_{mm}^{\oplus}=\begin{cases}0 & \text{if} \quad 1\leqslant m\leqslant\sigma,\\ D_{mm} & \text{if} \quad \sigma+1\leqslant m\leqslant N.\end{cases} \tag{50}$$

The 0 Hz modal terms being not accelerated, the preceding expression of $\mathbf{H}_{A\leftarrow B}$ can be given as an example of irreducible hybrid spectral formulation.

The analytical expression $\mathbf{P}_A(\mathbf{1}-\boldsymbol{\Pi}_M)(\lambda\boldsymbol{\Pi}+\mathbf{K})^{-1}(\mathbf{1}-\boldsymbol{\Pi}_M)^{\mathrm{T}}\mathbf{P}_B^{\mathrm{T}}$ of the inertia relief receptance is obviously of some mathematical interest and will probably serve to further theoretical developments. It can be applied to small finite element models in view of building benchmark tests to detect whether one or the other of the many "black boxes" that are devoted to modal corrections in modern engineering environments, correctly works or not. It has already been remarked however, that non-standard manipulations of huge matrices, as can be $\mathbf{K}$ or $\mathbf{M}$, cannot be recommended in practical applications. Projectors $\boldsymbol{\Pi}$, $\boldsymbol{\Pi}_M$, not only are huge matrices but also full ones. This is the reason why, in practice, a direct determination of the inertia relief receptance should be preferred to any other solution.

The computations can be performed as indicated in Fig. 4, with a preliminary condensation on the union $\Sigma=A\cup B\cup C\cup D\cup\cdots$ of preselected clusters of interest. The inertia relief receptance $\mathbf{I}_{\Sigma\leftarrow\Sigma}$ is quite similar to the static $\mathbf{G}_{\Sigma\leftarrow\Sigma}$ of Fig. 3. Column m is here the inertia relief response measured throughout Σ for a unit

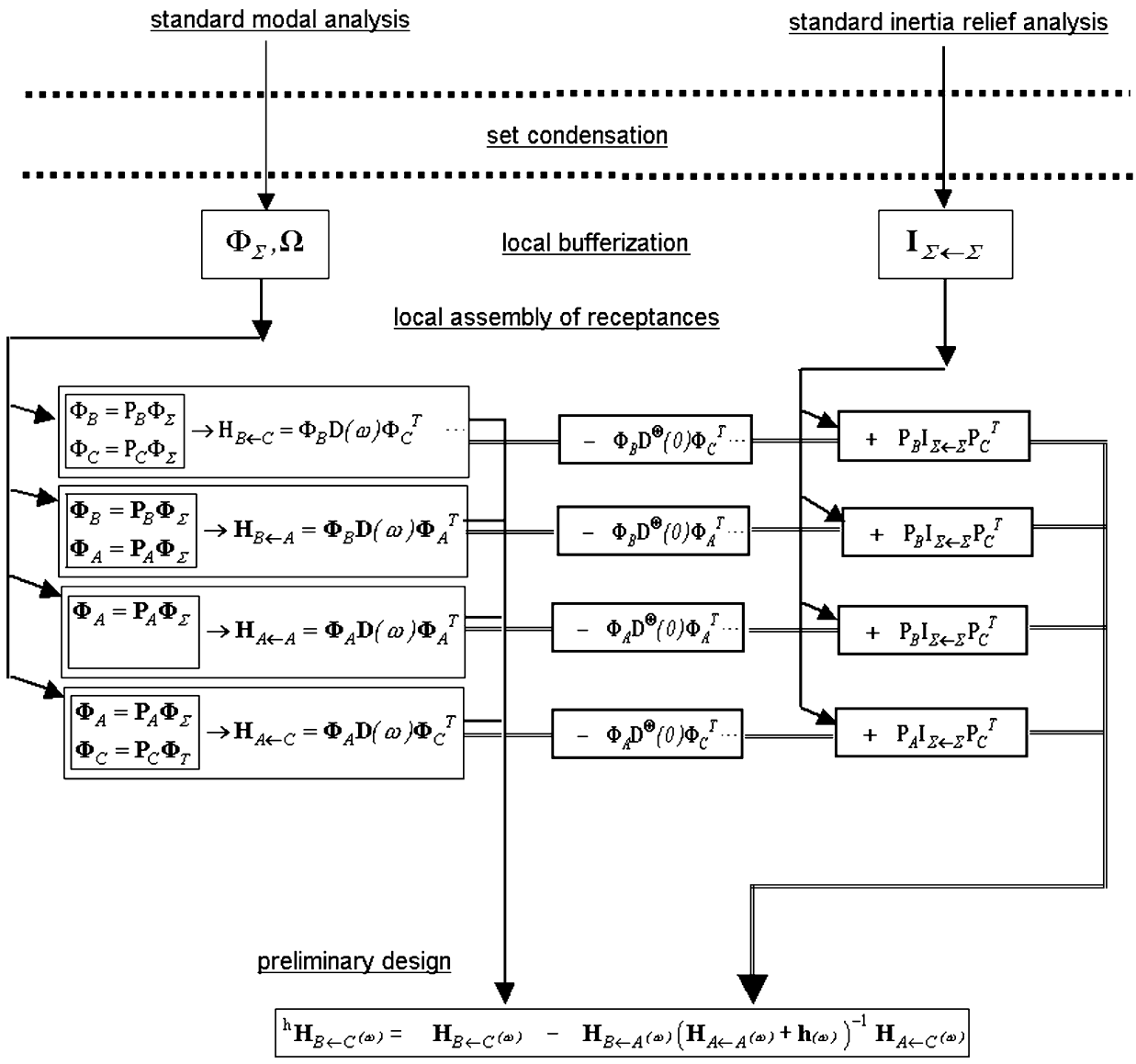

Fig. 4. Data flowchart for finite-dimensional singular floating systems.

excitation $\mathbf{f}$ at location m, that is to say the solution to

$$\begin{cases} \mathbf{K}\mathbf{x} = \mathbf{f} - \mathbf{f}_{\text{iner}}, \\ \boldsymbol{\Psi}_k^{\mathrm{T}}\mathbf{M}\mathbf{x} = 0, \quad k = 1, \ldots, \sigma. \end{cases} \tag{51}$$

There is theoretically no difficulty to implement such a solution. As a matter of fact, most finite element codes now propose their own versions of the inertia relief option. Moreover, special operations, such as assembling matrix $\mathbf{I}_{\Sigma\leftarrow\Sigma}$, can be programmed through the user-oriented language which, on the model of Nastran DMAP, is made available by the code. Unfortunately, in place of the correct "0 Hz filtration" above, earlier versions of the inertia relief option imposed a zero displacement on an arbitrary isostatic support. Because such variants are clearly not suitable for the present purpose, they must be discarded as soon as they are identified. It is worth noting that, in the proper task of identification, benchmark tests based on Eq. (49), on the model of the following example, can be of great interest.

2.4. Numerical examples

(a) *Free and fixed chains*: The inertia relief formula (49) has been numerically tested on the example of an aluminium bar in free longitudinal vibration. The bar is of length $L = 2\,\mathrm{m}$ and section $A = 10^{-4}\,\mathrm{m}^2$. As shown in Fig. 5, the discrete model is a 1D chain consisting of $\overline{N} = 100$ lumped masses m and $\overline{N} - 1 = 99$ springs k. Mechanical constants are given by $m = (\mu AL/\overline{N}) = 5.4 \times 10^{-3}\,\mathrm{kg}$ and $k = (EA/(L/\overline{N} - 1)) = 3.465 \times 10^{8}\,\mathrm{N\,m^{-1}}$, where $\mu = 2700\,\mathrm{kg\,m^{-3}}$ and $E = 7 \times 10^{10}\,\mathrm{N\,m^{-2}}$, respectively, correspond to the mass per unit of volume and the Young modulus of aluminium.

Table 1 lists the first 10 eigenfrequencies. The 0-frequency at the beginning of the list corresponds to the singularity of order $\sigma = 1$ that affects the considered one-dimensional (1D) floating system. The 0-eigenvalue is associated with a set of constant eigenvectors representing uniform translations of the chain. Because this

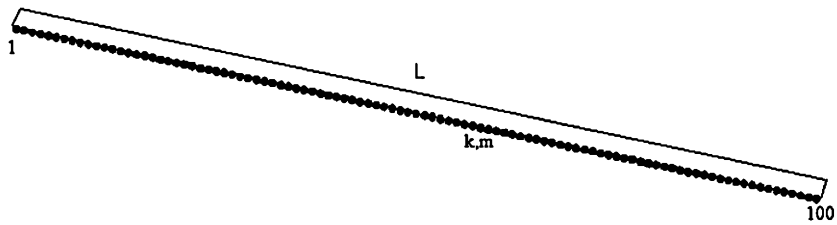

Fig. 5. One hundred-mass free–free chain for the simulation of the longitudinal vibrations of an aluminium rod.

Table 1
Eigenfrequencies of the free–free chain

Mode number	1	2	3	4	5	6	7	8	9	10
Frequency (Hz)	0	1272.9	2545.5	3817.4	5088.4	6358.1	7626.3	8892.6	10157	11418

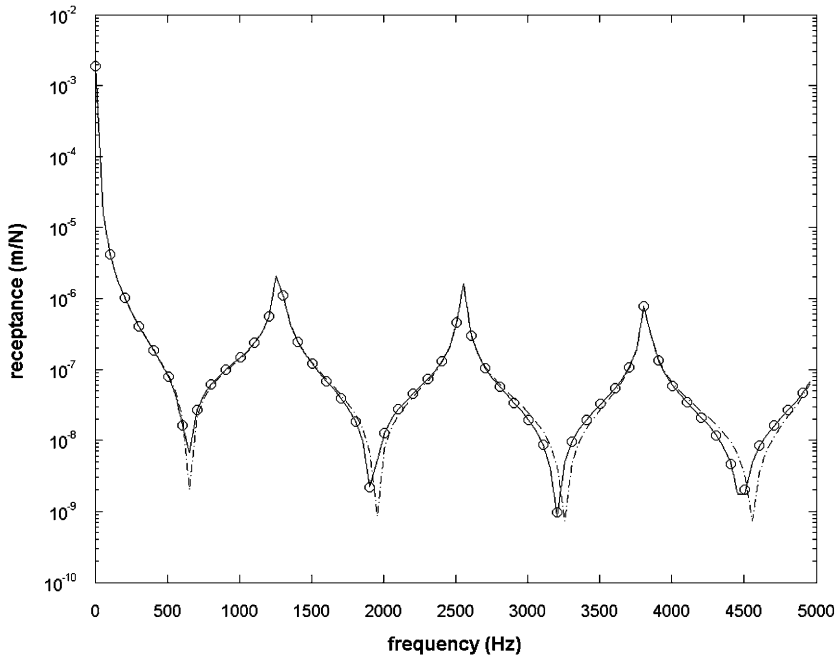

Fig. 6. Receptance at the free end of the free–free chain: ○ exact; — 10-mode inertia relief accelerated sum; - - - 10-mode ordinary sum.

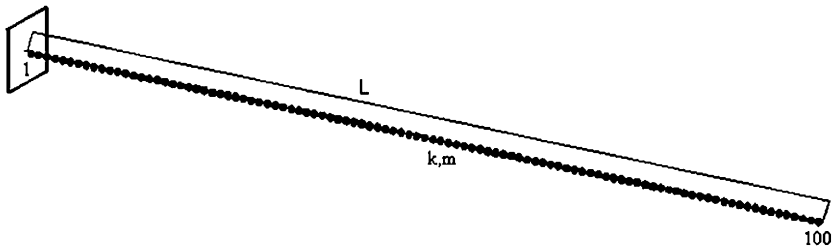

Fig. 7. Clamped–free chain.

Table 2
Eigenfrequencies of the clamped–free chain

Mode number	1	2	3	4	5	6	7	8	9	10
Frequency (Hz)	633.3	1899.7	3165.7	4430.9	5695	6957.7	8218.8	9477.8	10734	11989

simple set is but the kernel, Ker(**K**), of the stiffness matrix, there is no difficulty to compute the **Π**- and $\mathbf{\Pi}_M$-projectors of the general theory. As a result, Fig. 6 pictures the free end receptances that are obtained from a direct computation, a 10-mode ordinary superposition, and a 10-mode solution to Eq. (49). Clearly, the ordinary technique does not bear comparison with the inertia relief approach.

Fig. 7 gives a second example, obtained by fixing one end of the preceding chain. Although much more simple than the former, this example presents the interest of being the finite-dimensional counterpart of Kim and Kang's continuous rod. Table 2 lists the first 10 eigenfrequencies. The 0-frequency does not appear in the list, which is not surprising since the fixed chain is a regular mechanical system relevant to Section 2.1. Modal corrections are thus much easier than above and only require inversions in place of pseudo-inversions. Besides additional diagrams that will be explained in the next paragraph diagram d in Fig. 8 pictures the free end receptances that are obtained from a direct computation, a 10-mode ordinary superposition, and a 10-mode solution to Eq. (21). The conclusion is the same as before. However, since no general law can be inferred from a method that consists in comparing the results of two computations to decide for one technique or the other, the question of *a priori* error estimations must now be posed.

(b) *Spectrograms*: Modal expressions at any frequency ω, in free or fixed systems, have been found to be partial sums of general series whose remainders are those of ordinary and accelerated modal series:

$$\varepsilon_n = \sum_{m=n+1}^{\overline{N}} \frac{\Psi_m^2}{\omega_m^2 - \omega^2}, \quad \rho_n = \sum_{m=n+1}^{\overline{N}} \frac{\Psi_m^2}{\omega_m^2 - \omega^2} \frac{\omega^2}{\omega_m^2}, \tag{52}$$

where Ψ_m is the modal component of order m along the considered degree of freedom; and ω_m, the corresponding eigenfrequency. Prior to any heavy static or inertia relief solution, it can thus be proposed to check the convergence of ordinary and accelerated representations by plotting the partial sums

$$\Sigma_1 = \sum_{m=n_0}^{n} \frac{\Psi_m^2}{\omega_m^2 - \omega^2}, \quad \Sigma_2 = \sum_{m=n_0}^{n} \frac{\Psi_m^2}{\omega_m^2 - \omega^2} \frac{\omega^2}{\omega_m^2} \tag{53}$$

against the number $n \leqslant N$ of retained modes, in the most unfavourable case when ω is the maximum frequency of interest. Indeed, from a physicist's point of view, the slighter the slopes, $\mathrm{d}\Sigma_1/\mathrm{d}n$, $\mathrm{d}\Sigma_2/\mathrm{d}n$, grow, the smaller the remainders, ε_n, ρ_n, can be considered. Following the terminology of experimental physics, the preceding sums, or associated graphs, will be termed "spectrograms". Diagrams (a), (b), in Figs. 8 and 9, show first examples of Σ_1- and Σ_2-spectrograms. To avoid resonances and obtain smooth non-decreasing positive diagrams, it can be highly recommended to choose the lower index, n_0 , such that $\omega < \omega_{n0} < \omega_n$. This is not a difficulty, since, as far as consistent analyses are concerned, the maximum eigenfrequency, ω_N, is notably greater than the upper frequency, ω. That apart, it should be noted that curves are scaled down to the

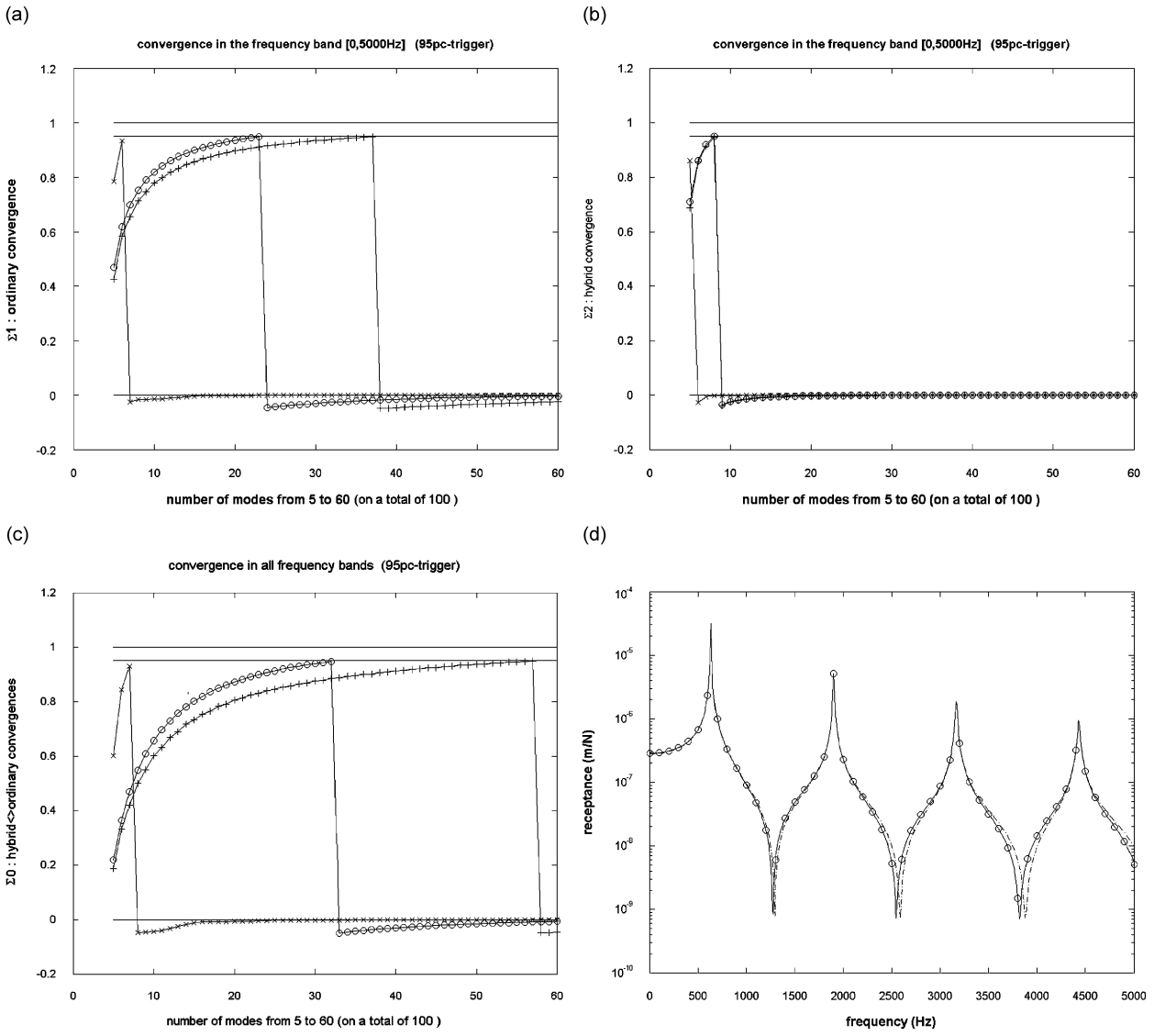

Fig. 8. Clamped–free chain (a)(b)(c) Σ_1-, Σ_2-, Σ_0-spectrograms (○ receptance at the end of the rod; + receptance in the middle of the rod; × 10-point average receptance at the free end). (d) Receptance at the free end (○ exact; — 10-mode accelerated sum; - - - 10-mode ordinary sum).

standard interval [0,1] in order to be easily compared one with the other. Lastly, there is few to comment on the reason why crossing a predefined threshold triggers off a unit downward shift, except that this graphical trick has been found to make a quick count of modes possible.

Owing to the fact that ordinary and corrected sums of order n differ by the constant

$$\varepsilon_n(0) = \sum_{m=n+1}^{\overline{N}} \frac{\Psi_m^2}{\omega_m^2}, \tag{54}$$

a third spectrogram is introduced on diagrams (c)

$$\Sigma_0 = \sum_{m=n_0}^{n} \frac{\Psi_m^2}{\omega_m^2}, \tag{55}$$

whose "stabilization" , in the above sense, means that static corrections are of minor interest.

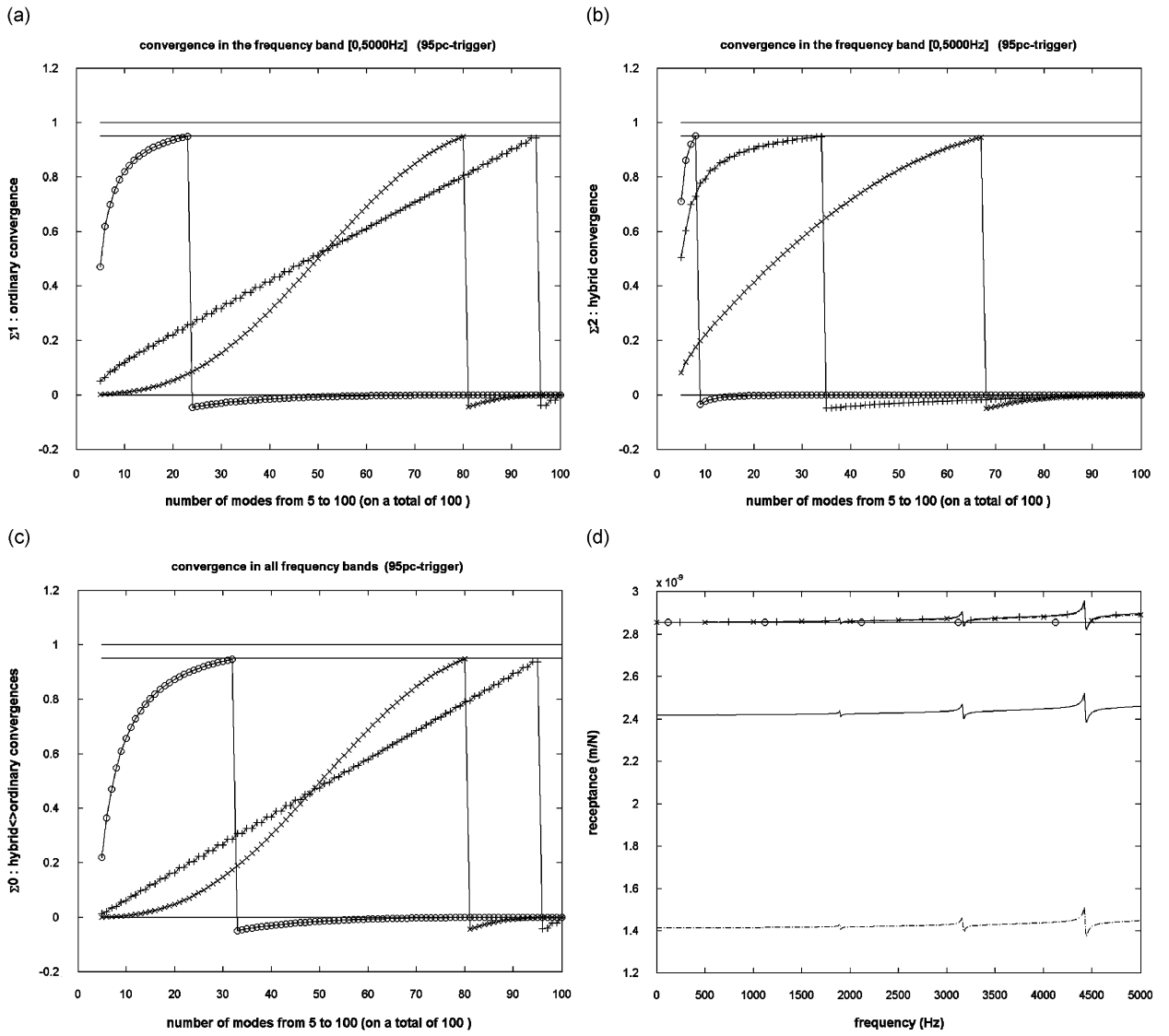

Fig. 9. Clamped–free chain (a)(b)(c) Σ_1-, Σ_2-, Σ_0-spectrograms (○ receptance at the end of the chain ; + local flexibility in the middle of the chain; × local flexibility at the free end). (d) Receptance at the free end (○ exact; - - - 50-mode ordinary sum, — 70-mode ordinary sum, ×-50 mode accelerated sum, + 70-mode accelerated sum).

Although the phenomena could be imagined as depending exclusively on the frequency range, Figs. 8 and 9 show how various dofs respond differently to modal truncation.

(c) *Classification of dofs*: Three series of spectrograms are plotted in Fig. 8: the first series, on diagram (a), consists of three Σ_1-spectrograms; the second series, on diagram (b), shows three Σ_2-spectrograms; and, lastly, diagram (c) shows a third series of three Σ_0-spectrograms. Inside each series, markers "o", "+", and "×", respectively, indicate the receptance, $\mathbf{x}_{100}/\mathbf{f}_{100}$, at the end of the chain; the receptance, $\mathbf{x}_{50}/\mathbf{f}_{50}$, in the middle of the chain; a little more complicated 10-point average end-receptance, that can be defined as x/f, with $x = (\mathbf{x}_{100} + \mathbf{x}_{99} + \cdots \mathbf{x}_{91})/10$, and $\mathbf{f}_{100} = \mathbf{f}_{99} = \cdots \mathbf{f}_{91} = f/10$. Diagrams (a), (b), (c) in Fig. 9, are of the same nature as above. Marker "o" still designates the receptance at the free end, which is taken as a reference. Markers "+" and "×" correspond to two flexibilities x/f, that are evaluated, respectively: at the end of the chain, with $x = \mathbf{x}_{100} - \mathbf{x}_{99}$, and $\mathbf{f}_{100} = -\mathbf{f}_{99} = f$; and in the middle of the chain, with $x = \mathbf{x}_{50} - \mathbf{x}_{49}$,

and $\mathbf{f}_{50} = -\mathbf{f}_{49} = f$. It is worth noting that the two first receptances of Fig. 8 refer to "primary" dofs, while the third receptance relates to $x = (\mathbf{x}_{100} + \mathbf{x}_{99} + \cdots \mathbf{x}_{91})/10$, which is an example of "least squares" secondary dof. In turn, the two flexibilities considered in Fig. 9 relate to "finite differences" secondary dofs.

Prior to any discussion, it seems quite necessary: first, to explain how to synthesize the matrices, $\mathbf{P}$, that give secondary dofs, or vectors of such entities, as linear combinations, $\boldsymbol{\xi} = \mathbf{P}\mathbf{x}$, of primary ones; second, to comment on using the same formulae, $\mathbf{H}_{A\leftarrow B}(\omega) = \mathbf{P}_A\mathbf{H}(\omega)\mathbf{P}_B^{\mathrm{T}}$, for secondary receptances as for primary ones. Concerning the first point, it can be remarked that the 2 flexibilities in Fig. 9 can indeed be defined by finite differences matrices, $\mathbf{P} = [0 \cdots 1 \cdots 0 \cdots -1 \cdots 0]$, with 1 and -1 at the adequate locations. To illustrate now the construction of least squares dofs, it is possible to consider a group, G, of P primary dofs, and try to express the displacement on G, $\mathbf{x}_G$, as a combination of $Q < P$ pre-selected displacements, the coefficients being precisely the considered secondary dofs. If $\mathbf{S}_G$ denotes the corresponding $P \times Q$ shape-matrix, the problem consists in finding the Q-vector, ξ, that minimizes $||\mathbf{S}_G\boldsymbol{\xi} - \mathbf{x}_G||$. Appendix A defines the solution to this problem as $\boldsymbol{\xi} = \mathbf{P}_G\mathbf{x}_G$, with $\mathbf{P}_G = (\mathbf{S}_G^{\mathrm{T}}\mathbf{S}_G)^{-1}\mathbf{S}_G^{\mathrm{T}}$, and it remains to complete matrix $\mathbf{P}_G$ by an adequate number of 0-columns, to bring the Q-vector of secondary dofs to the announced form, $\boldsymbol{\xi} = \mathbf{P}\mathbf{x} = [\mathbf{P}_G \cdots \mathbf{0} \cdots]\mathbf{x}$. For example, the 10-point average displacement above, $x = (\mathbf{x}_{100} + \mathbf{x}_{99} + \cdots \mathbf{x}_{91})/10$, is indeed the least squares mean rigid motion at the end of the chain, with $\mathbf{S}_G$, a 10-vector of 1's , and $(\mathbf{S}_G^{\mathrm{T}}\mathbf{S}_G)^{-1}\mathbf{S}_G^{\mathrm{T}} = (1/10)[1\ 1 \cdots 1]$. The next step looks like reading a matrix by columns, after it has been filled up by rows: the point is indeed to make dual variables $\boldsymbol{\varphi}$ explicit, together with algebraic identities $\langle \mathbf{P}\mathbf{x}|\varphi\rangle \equiv \langle \mathbf{x}|\mathbf{P}^{\mathrm{T}}\varphi\rangle$. It becomes then possible to explain the role of adjoint matrices by comparing these relations to the physical balance conditions $\langle \boldsymbol{\xi}|\boldsymbol{\varphi}\rangle \equiv \langle \mathbf{x}|\mathbf{f}\rangle$ that can be imposed on energy-conservative least squares "best approximations", or that are invoked in finite differences computations by virtue of the virtual work principle. The comparison results in $\mathbf{f} = \mathbf{P}^{\mathrm{T}}\varphi$ with the first consequence that secondary receptances obey composition rules of the type $\varphi_B \xrightarrow{\mathbf{P}_B^{\mathrm{T}}} \mathbf{f} \xrightarrow{\mathbf{H}} \mathbf{x} \xrightarrow{\mathbf{P}_A} \boldsymbol{\xi}_A$, and take therefore the announced canonical form, $\mathbf{P}_A\mathbf{H}(\omega)\mathbf{P}_B^{\mathrm{T}}$. Another consequence is that secondary dofs can be handled by means of modal matrices $\boldsymbol{\Phi}_A = \mathbf{P}_A\boldsymbol{\Phi}$.

Despite this common algebraic structure, a great diversity can be observed, that takes its origin in physical reasons behind the numerical model. For example, the 10-point average displacement at the free extremity of the chain in Fig. 8 is seen to be easily calculable with a limited number of modes, and even with an ordinary modal superposition. Indeed, alternations of signs in the primary modal components, make that high order modes with wavelengths notably shorter than the 10-point region, cannot significantly contribute to the final result. Decisive contributions being concentrated on a few lower order modal terms, the considered dof can be said of "small modal depth", or, equivalently, be called a "shallow" dof. Measuring the modal depth can be of great interest in engineering applications, since least squares variables are intended to deliver rapid and robust evaluations of simplified models of structural modifications.

By contrast, the two flexibilities in Fig. 9, are examples of "deep" dofs. First, Σ_1-spectrograms on diagram (a) reveal the inability of ordinary modal sums to reconstitute the local flexibilities, either at the end or in the middle of the chain (with the somehow amazing observation that the comparison between the end- and the mid-flexibilities is largely in disfavour of the latter). Second, Σ_2- and Σ_0-spectrograms show that considerably better results can be obtained by using accelerated series. The end flexibility being nevertheless much more difficult to obtain than the middle one, it is suggested to describe such a dof as "extremely deep". The prognostication is confirmed on diagram (d), where various ordinary or accelerated modal sums can be compared with the exact value $k^{-1} = (3.465 \times 10^8)^{-1} = 2.886 \times 10^{-9}\,\mathrm{m\,N^{-1}}$. In the considered [0,5000 Hz] frequency range, the usual rule would suggest to retain modes up to twice the maximum frequency, that is to say, up to10,000 Hz. The 9th and 10th eigenfrequencies being respectively found in Table 2 at 10,734 and 11,989 Hz, about 10 modes should be thus retained. It is clear that this choice is notably insufficient for the kind of dofs under examination.

The difficulty has already been identified as resulting from a modal boundary discontinuity in the underlying infinite-dimensional formulation. According to the aforementioned discussion, there is nothing surprising about that accelerated series deliver considerably better results than ordinary ones. This answer cannot however be considered as definitive unless direct studies are carried out, in an appropriate infinite-dimensional context.

3. On the so-called inability of free interface modes in representing stress resultants near the free interface

3.1. Regarding a recent paper by Kim and Kang [20]

A recurrent question in spectral theory is to control what happens when zero modal quantities, f_m, are requested, by mathematical developments themselves, to satisfy a non-zero boundary condition $F = \Sigma\gamma_m f_m$. Such a question dilutes itself in finite-dimensional approximations, and can only be observed on the infinite-dimensional differential equations. In a recent paper, from which the title of the present section has been taken, Kim and Kang focused on the longitudinal vibrations of a fixed–free bar driven by a force F, as illustrated in Fig. 10. The difficulty at the loaded end, $x = L$, lies in that zero modal derivatives $\psi'_m(L) = 0$ are intended to express the inhomogeneous boundary condition

$$F = EA\Sigma\alpha_m\psi'_m(L). \tag{56}$$

There is some exaggeration in speaking of "impossibility" or "inability" as the authors do. The detailed drawing of the Gibbs oscillation at the end of Kim and Kang's rod in Fig. 2, illustrates how homogeneous modes can bring inhomogeneous boundary conditions under mathematical control.

Boundary discontinuities and modal truncation have been recognized in Section 1.1 as intimately intricate topics. The present section precisely shows how using the method of orthocomplement to the solution of Kim and Kang's problem, eliminates the Gibbs phenomenon, and produces improved accelerated modal representations.

It is worth noting that submitting an ordinary spectral series to the 0-shift, $f(\omega) = f(0) + f(\omega) - f(0)$, formally leads to the latter result. The subtlety of the present proof, however, lies in that no reference is made to the litigious serial summation $\sum_{m=1}^{\infty}\langle\psi_m|U\rangle\psi_m(x)$.

3.2. Formulation of the problem

For a harmonic excitation force $Fe^{i\omega t}$ the steady-state longitudinal response can be written $u(x,t) = U(x)e^{i\omega t}$, provided $U(x)$ be the solution to the boundary problem

$$U''(x) + \frac{\omega^2}{c^2}U(x) = 0, \quad U(0) = 0, \quad U'(L) = \frac{F}{EA}, \tag{57}$$

where $c = \sqrt{E/\mu}$ denotes the wave propagation velocity in the bar; ω, the angular frequency; μ the density; E the Young's modulus; A, L the material area and length of the bar; and where, on evidence, quotes designate derivations $\mathrm{d}/\mathrm{d}x$ with respect to the abscissa along the rod.

The clamped–free bar normal modes, ψ_m, and eigenfrequencies, ω_m, satisfy the following equations:

$$\psi''_m(x) + \frac{\omega_m^2}{c^2}\psi_m(x) = 0,\ \psi_m(0) = 0,\ \psi'_m(L) = 0 \tag{58}$$

with

$$\omega_m = \frac{c}{L}\left(-\frac{\pi}{2} + m\pi\right), \quad \psi_m = \sqrt{\frac{2}{\mu AL}}\sin\left(-\frac{\pi}{2} + m\pi\right)\frac{x}{L}. \tag{59}$$

Because

$$\int_0^L \sin^2\left(-\frac{\pi}{2} + m\pi\right)\frac{x}{L}\,\mathrm{d}x = \frac{1}{2}L - \frac{1}{2}\int_0^L \cos(2m-1)\frac{\pi x}{L}\,\mathrm{d}x = \frac{L}{2}, \tag{60}$$

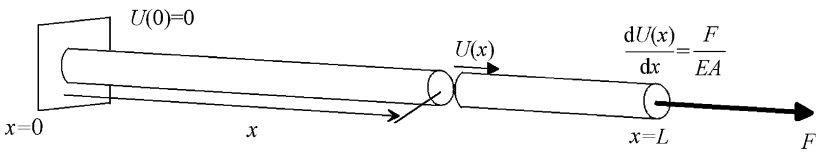

Fig. 10. The Kim–Kang bar in compression.

it can easily be verified that the normalization coefficient $\sqrt{2/(\mu AL)}$ is adjusted in such a way that the ψ_m form an orthonormal system for the inner product $\langle f|g\rangle = \int_{[0,L]} fg\mu A\,\mathrm{d}x$. The reason why to include the mass μA per unit length in the differential element will appear later. Let for the moment the response function U be projected on the first N modes

$$U(x) = \sum_{m=1}^{N} \langle \Psi_m | U\rangle \psi_m(x) + \varepsilon_N, \quad \langle \varepsilon_N | \psi_m\rangle = 0,\ m = 1, \ldots, N \tag{61}$$

with an orthocomplement ε_N, that dispenses from taking part in any quarrel over whether it is possible or not to approximate the boundary condition $U'(L) = F(EA)^{-1}$ by means of the homogeneous modal boundary conditions $\psi'_m(L) = 0$.

Green formulae, that in the considered 1D example merely result from adequate integrations by parts, can be written for any pair of regular functions

$$\begin{aligned} \langle f''|g\rangle &= \mu A \int_{[0,L]} f'' g\,\mathrm{d}x = \mu A \int_{[0,L]} \frac{\mathrm{d}}{\mathrm{d}x}(f'g)\,\mathrm{d}x - \mu A \int_{[0,L]} f'g'\,\mathrm{d}x = \mu A[f'g]_0^L - \mu A \int_{[0,L]} f'g'\,\mathrm{d}x \\ \langle f''|g\rangle &- \langle g''|f\rangle = \mu A[f'g - g'f]_0^L \end{aligned} \tag{62}$$

and are the key for the computation of coefficients $\langle \psi_m | U\rangle$ in formula (61). As a matter of fact the substitution of conditions (57) and (58) in the second Green formula

$$\langle U''|\psi_m\rangle - \langle \psi''_m|U\rangle = \mu A[U'\psi_m - \psi'_m U]_0^L \tag{63}$$

immediately brings

$$\frac{(\omega_m^2 - \omega^2)}{c^2}\langle U|\psi_m\rangle = \mu A[U'(L)\psi_m(L) - U(L)\psi'_m(L) - U'(0)\psi_m(0) - U(0)\psi'_m(0)]. \tag{64}$$

The μA weight that was put on the scalar product can now be justified by the elimination of all physical constants in the definitive result:

$$\langle U|\psi_m\rangle = \frac{\mu A c^2 \psi_m(L)}{(\omega_m^2 - \omega^2)}\frac{F}{EA} = \frac{\mu c^2}{E}\frac{\psi_m(L)F}{(\omega_m^2 - \omega^2)} = \frac{\psi_m(L)F}{(\omega_m^2 - \omega^2)}. \tag{65}$$

The simplicity of the result marks that the weighted inner product is the exact counterpart of the finite-dimensional M-product of Section 2, which indeed is not very surprising.

One has finally

$$U(x) = \sum_{m=1}^{N} \frac{\psi_m(x)\psi_m(L)}{(\omega_m^2 - \omega^2)} F + \varepsilon_N \tag{66}$$

from which the orthocomplement has now to be evaluated.

3.3. Application of the method of orthocomplement

(a) *Forward step*: A double derivation of Eq. (66) with respect to the spatial variable x, brings, with the aid of Eqs. (57) and (58)

$$\begin{aligned} \varepsilon''_N &= U'' - \sum_{m=1}^{N} \frac{F\psi_m(L)}{(\omega_m^2 - \omega^2)}\psi''_m(x) = -\frac{\omega^2}{c^2}U(x) + \sum_{m=1}^{N} \frac{F\psi_m(L)}{(\omega_m^2 - \omega^2)}\frac{\omega_m^2}{c^2}\psi_m(x) \\ &= -\frac{\omega^2}{c^2}\varepsilon_N - \frac{\omega^2}{c^2}\sum_{m=1}^{N} \frac{F\psi_m(L)}{(\omega_m^2 - \omega^2)}\psi_m(x) + \sum_{m=1}^{N} \frac{F\psi_m(L)}{(\omega_m^2 - \omega^2)}\frac{\omega_m^2}{c^2}\psi_m(x) = -\frac{\omega^2}{c^2}\varepsilon_N + \sum_{m=1}^{N} \frac{F\psi_m(L)}{c^2}\psi_m(x). \end{aligned}$$

The orthocomplement ε_N therefore satisfies

$$\varepsilon_N'' + \frac{\omega^2}{c^2}\varepsilon_N = \sum_{m=1}^{N} \frac{F}{c^2}\psi_m(L)\psi_m(x),\ \varepsilon_N(0) = 0,\ \varepsilon_N'(L) = \frac{F}{EA}, \tag{67}$$

where the boundary conditions are easily derived from Eqs. (57), (58) and (66).

As usual, those equations seem much more complicated to solve than the original ones and only need to be divided into two parts:

$$\varepsilon_N = \eta_N + \rho_N \begin{cases} \eta_N'' = \sum\limits_{m=1}^{N} \dfrac{F}{c^2}\psi_m(L)\psi_m(x),\ \eta_N(0) = 0,\ \eta_N'(L) = \dfrac{F}{EA} \quad \text{(A)}, \\ \rho_N'' + \dfrac{\omega^2}{c^2}\rho_N = -\dfrac{\omega^2}{c^2}\eta_N,\ \rho_N(0) = 0,\ \rho_N'(L) = 0 \quad \text{(B)}. \end{cases} \tag{68}$$

By the change of unknown

$$\theta(x) = \eta_N(x) - \frac{F}{EA}x \tag{69}$$

problem (A) turns to

$$\theta'' = \sum_{m=1}^{N} \frac{F}{c^2}\psi_m(L)\psi_m(x),\ \theta(0) = 0,\ \theta'(L) = 0. \tag{70}$$

A direct computation shows that a solution to the above equations, is given by

$$\theta^*(x) = \sum_{m=1}^{N} \frac{F}{\omega_m^2}\psi_m(L)\psi_m(x). \tag{71}$$

It is the only one since the difference, δ, of two solutions must verify

$$\delta''(x) = 0,\ \delta(0) = 0,\ \delta'(L) = 0,$$

that is to say $\delta(x) = ax + b$ with $a = b = 0$.

Consequently, the only solution to problem (A) is

$$\eta_N(x) = \frac{F}{EA}x - \sum_{m=1}^{N} \frac{F}{\omega_m^2}\psi_m(L)\psi_m(x). \tag{72}$$

The solution to problem (B) has now to be found.

(b) *Coordination step*: In contrast to the initial formulation, problem (B) does not present any modal boundary discontinuity at $x = L$. As a first consequence, the Gibbs phenomenon will not affect the solution. Moreover, ρ_N, being the solution to a smooth problem, can be easily written as an infinite series

$$\rho_N(x) = \sum_{m=1}^{\infty} \langle \rho_N | \psi_m \rangle \psi_m(x). \tag{73}$$

As in the finite-dimensional examples of Section 2, the first step of computation now consists in determining the modal projections $\langle \psi_k | \rho_N \rangle$ as functions of the projections $\langle \psi_k | \eta_N \rangle$. This can be achieved by eliminating the derivatives and boundary values of ρ_N and ψ_k between Eqs. (68), (58) and the second Green formula

$$\langle \rho_N'' | \psi_k \rangle - \langle \rho_N | \psi_k'' \rangle = \mu A[\rho_N'\psi_k - \rho_N\psi_k']_0^L. \tag{74}$$

This brings

$$-\frac{\omega^2}{c^2}\langle \rho_N | \psi_k \rangle - \frac{\omega^2}{c^2}\langle \eta_N | \psi_k \rangle + \frac{\omega_k^2}{c^2}\langle \rho_N | \psi_k \rangle = \mu A[\rho_N'(L)\psi_k(L) - \rho_N(L)\psi_k'(L) - \rho_N'(0)\psi_k(0) + \rho_N(0)\psi_k'(0)] = 0$$

and, after some rearrangements

$$\langle \rho_N | \psi_k \rangle = \frac{\omega^2}{\omega_k^2 - \omega^2} \langle \eta_N | \psi_k \rangle. \tag{75}$$

To compute $\langle \eta_N | \psi_k \rangle$, a similar elimination between Eqs. (68), (58) and the second Green formula

$$\langle \eta_N'' | \psi_k \rangle - \langle \eta_N | \psi_k'' \rangle = \mu A [\eta_N' \psi_k - \eta_N \psi_k']_0^L \tag{76}$$

yields

$$\begin{aligned} &\sum_{m=1}^{N} \frac{F}{c^2} \psi_m(L) \langle \psi_m | \psi_k \rangle + \frac{\omega_k^2}{c^2} \langle \eta_N | \psi_k \rangle \\ &\quad = \mu A [\eta_N'(L)\psi_k(L) - \eta_N(L)\psi_k'(L) - \eta_N'(0)\psi_k(0) + \eta_N(0)\psi_k'(0)] \\ &\quad = \mu A \frac{F}{EA} \psi_k(L) = \frac{F}{c^2} \psi_k(L) \end{aligned}$$

It is thus possible to write

$$\langle \eta_N | \psi_k \rangle = \frac{F}{\omega_k^2} \left[\psi_k(L) - \sum_{m=1}^{N} \psi_m(L) \langle \psi_m | \psi_k \rangle \right] = \begin{cases} 0 & \text{if} \quad 1 \leqslant k \leqslant N \\ \dfrac{F \psi_k(L)}{\omega_k^2} & \text{if} \quad N+1 \leqslant k \end{cases} \tag{77}$$

The modal components of ρ_N can then be found by substituting for $\langle \eta_N | \psi_k \rangle$ from Eqs. (77) into (75).

(c) *Backward step*: Assembling the ordinary modal sum, the pseudo-static solution (72) and the spectral development (73) of ρ_N, finally yields

$$U(x) = \left\{ \sum_{m=1}^{N} \frac{F}{(\omega_m^2 - \omega^2)} \psi_m(L) \psi_m(x) \right\} + \frac{F}{EA} x - \sum_{m=1}^{N} \frac{F}{\omega_m^2} \psi_m(L) \psi_m(x) + \left\{ \sum_{m=N+1}^{\infty} \frac{\omega^2}{\omega_m^2} \frac{F}{(\omega_m^2 - \omega^2)} \psi_m(L) \psi_m(x) \right\}. \tag{78}$$

This expression can easily be simplified to the "accelerated" representation

$$U(x) = \frac{F}{EA} x + \sum_{m=1}^{\infty} \frac{\omega^2}{\omega_m^2} \frac{F}{(\omega_m^2 - \omega^2)} \psi_m(L) \psi_m(x). \tag{79}$$

The corresponding approximation of the tension inside the rod

$$T(x) \simeq F + EA \sum_{m=1}^{N} \frac{\omega^2}{\omega_m^2} \frac{F}{(\omega_m^2 - \omega^2)} \psi_m(L) \psi_m'(x) \tag{80}$$

has been tested on the aluminium bar of Section 2.4, whose mechanical properties and geometric dimensions are: Young's modulus $E = 7e^{10}\,\mathrm{N/m^2}$; mass density $\mu = 2700\,\mathrm{kg/m^3}$; length $L = 2\,\mathrm{m}$; cross section area $A = 0.0001\,\mathrm{m^2}$. The result at 4000 Hz, for 10 modes (see Table 3), is compared in Fig. 11 to the

Table 3
Eigenfrequencies of the clamped–free bar

Mode number	1	2	3	4	5	6	7	8	9	10
Frequency (Hz)	636.5	1909.4	3182.3	4455.3	5728.2	7001.2	8274.1	9547	10820	12093

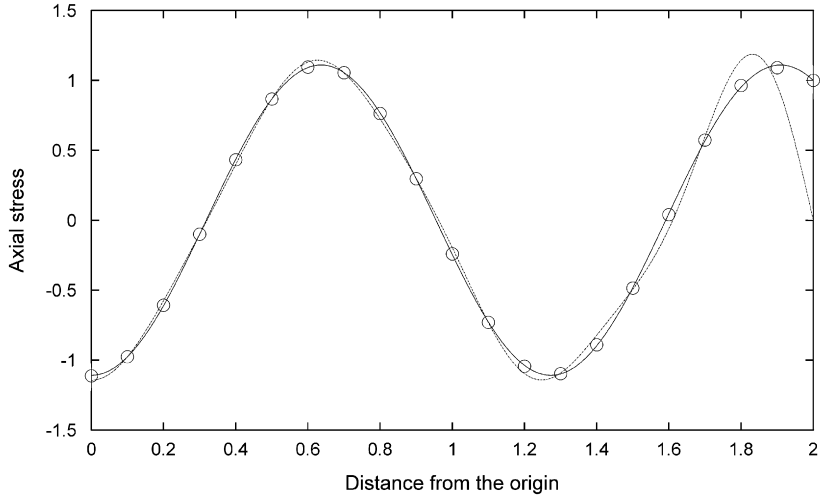

Fig. 11. Axial stress in the clamped–free bar subjected to a prescribed force: ---- 10-mode ordinary modal sum, —— 10-mode accelerated modal sum, ○ ○ ○ analytical solution.

analytical solution

$$T(x) = EAU'(x) \quad \text{with} \quad U(x) = \frac{cF}{EA\omega \cos \frac{\omega}{c}L} \sin \frac{\omega x}{c} \tag{81}$$

and to the ill-behaving ordinary modal sum of the same order.

Although the stress has not been put on functional analysis, it should be clear that the quality of results could be explained by the fact that general Green formulae are not blurred by apparent pointwise discontinuities.

3.4. The case of natural boundary discontinuities

To confront the method with a natural boundary discontinuity, it can be now supposed that the rod is submitted to an imposed displacement U_0 at $x = 0$, with a free condition, $T = 0$ at $x = L$. Equations of motion can be written

$$U'(x) + \frac{\omega^2}{c^2} U(x) = 0, \quad U(0) = 1, \quad U'(L) = 0. \tag{82}$$

The modes and eigenfrequencies, ψ_m, ω_m, to be considered are the same as before and the application of Green's formula to the pair U, ψ_m gives the modal projections as

$$\langle \psi_m | U \rangle = \frac{EAU_0}{\omega_m^2 - \omega^2} \psi'_m(0). \tag{83}$$

From this, the orthocomplement $\varepsilon_N(x)$ is defined by

$$U(x) = \sum_{m=1}^{N} \frac{EAU_0}{\omega_m^2 - \omega^2} \psi'_m(0)\psi_m(x) + \varepsilon_N(x) \tag{84}$$

and appears after some calculations as the solution to the boundary problem

$$\varepsilon''_N + \frac{\omega^2}{c^2} \varepsilon_N = \sum_{m=1}^{N} \mu A U_0 \psi'_m(0)\psi_m(x), \quad \varepsilon_N(0) = U_0, \quad \varepsilon'_N = 0. \tag{85}$$

Splitting up (85) into two sub-problems results in

$$\varepsilon_N = \eta_N + \rho_N \begin{cases} \eta_N'' = \sum_{m=1}^{N} \mu A U_0 \psi_m'(0)\psi_m(x), \quad \eta_N(0) = U_0,\ \eta_N'(L) = 0 \quad \text{(A)}, \\ \rho_N'' + \dfrac{\omega^2}{c^2}\rho_N = -\dfrac{\omega^2}{c^2}\eta_N, \quad \rho_N(0) = 0, \quad \rho_N'(L) = 0 \quad \text{(B)}. \end{cases} \tag{86}$$

By the change of unknown $\eta_N = U_0 + \zeta$, problem (A) becomes

$$\zeta'' = -\sum_{m=1}^{N} \mu A U_0 \psi_m'(0)\psi_m(x), \quad \zeta(0) = 0, \quad \zeta'(L) = 0. \tag{87}$$

Uniqueness of the solution results from the same argumentation as before. Searching for ζ as a linear combination of ψ_m, $m = 1,\ldots,N$, then leads to

$$\eta_N = U_0 - \sum_{m=1}^{N} \frac{EAU_0}{\omega_m^2}\psi_m'(0)\psi_m(x). \tag{88}$$

Problem (B) can now be solved in writing down the second Green formulae

(i) for the pair ρ_N, ψ_m: $\langle \rho_N | \psi_k \rangle = (\omega^2/(\omega_k^2 - \omega^2))\langle \eta_N | \psi_k \rangle$;
(ii) for the pair η_N, ψ_m:

$$\langle \eta_N | \psi_k \rangle = \frac{1}{\omega_k^2}\left[EAU_0\psi_k'(0) - \sum_{m=1}^{N} EAU_0\delta_{km}\psi_k'(0) \right] = \begin{cases} 0 \quad \text{if} \quad 1 \leqslant k \leqslant N, \\ \dfrac{EAU_0}{\omega_k^2}\psi_k'(0) \quad \text{if} \quad N+1 \leqslant k. \end{cases} \tag{89}$$

It comes from successive eliminations that

$$\langle \rho_N | \psi_k \rangle = \begin{cases} 0 \quad \text{if} \quad 1 \leqslant k \leqslant N, \\ \dfrac{\omega^2}{\omega_k^2}\dfrac{EAU_0}{\omega_k^2 - \omega^2}\psi_k'(0) \quad \text{if} \quad N+1 \leqslant k. \end{cases} \tag{90}$$

Combining Eqs. (83), (88) and (90) then yields the hybrid spectral solution

$$U(x) = \sum_{m=1}^{N} \frac{EAU_0}{\omega_m^2 - \omega^2}\psi_m'(0)\psi_m(x) + U_0 - \sum_{m=1}^{N} \frac{EAU_0}{\omega_m^2}\psi_m'(0)\psi_m(x) + \sum_{m=N+1}^{\infty} \frac{\omega^2}{\omega_m^2}\frac{EAU_0}{\omega_m^2 - \omega^2}\psi_m'(0)\psi_m(x). \tag{91}$$

The expression can be simplified to the minimum accelerated form

$$U(x) = U_0 + EAU_0 \sum_{m=1}^{\infty} \frac{\omega^2}{\omega_m^2}\frac{\psi_m'(0)}{\omega_m^2 - \omega^2}\psi_m(x). \tag{92}$$

Fig. 12 shows a comparison between a 10-mode approximation of expression (92), an ordinary spectral sum and the analytical solution

$$U(x) = U_0\left(\cos\frac{\omega x}{c} + tg\frac{\omega L}{c}\sin\frac{\omega x}{c} \right). \tag{93}$$

At the considered stage of approximation, the ordinary sum looks quite inaccurate, and the number of modes is too low for the Gibbs phenomenon to appear. The Gibbs oscillation of a 100-mode ordinary sum can indeed be detected on the much more refined drawing of Fig. 13; it is of some interest to remark that the phenomenon does not occur unless the boundary condition begins to be correctly taken into account.

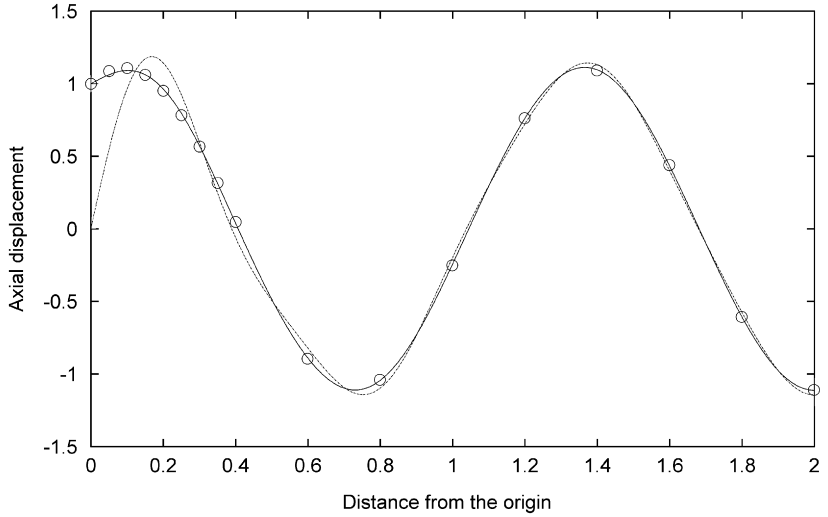

Fig. 12. Axial displacement in the clamped–free bar subjected to a prescribed displacement: ---- 10-mode ordinary modal sum, —— 10-mode accelerated modal sum, ○ ○ ○ analytical solution.

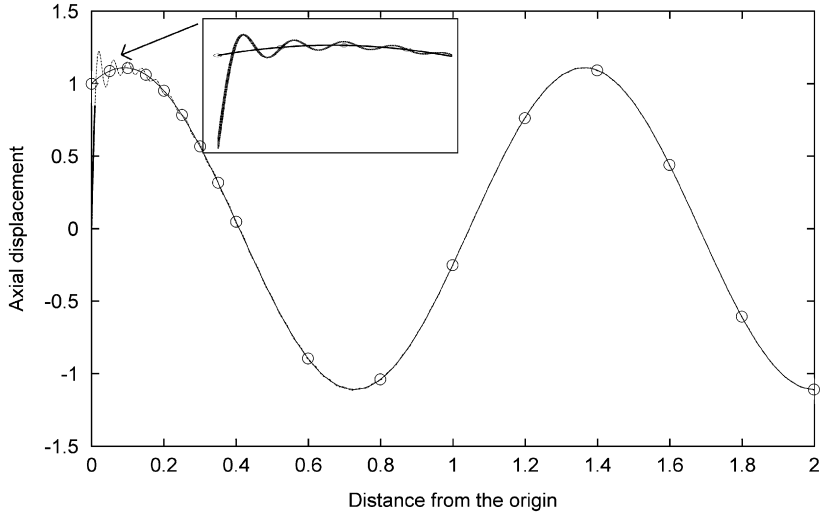

Fig. 13. Axial displacement, clamped–free bar subjected to a prescribed displacement: ---- 100-mode ordinary modal sum, —— 100-mode accelerated modal sum, ○ ○ ○ analytical solution.

4. Acoustic receptance at the boundary of a rigid cavity

4.1. Basic problem

Systems including acoustic parts are of a great practical importance, and are generally analysed by means of heavy boundary element methods. For the discussion and effective design of such systems, it should be very attractive to introduce impedance relations, $\mathbf{p}_B = \mathbf{Z}_{B\leftarrow A}\mathbf{v}_A$, describing the acoustic pressure, $\mathbf{p}_B$, over a region B when the velocity $\mathbf{v}_A$ is imposed on a region A of the boundary. That way of reasoning from displacements to efforts being induced by the exchange between primal and dual variables that characterizes the basic Helmholtz equation, it can be easily seen that acoustic finite element modal analyses should be able to deliver such quantities. The approach has however to face two major difficulties: first, the boundary discontinuity that

affects the modal superposition; and second, the Helmholtz singularity at 0 Hz, that complicates modal corrections.

It is thus proposed in the present section to analyse, from both theoretical and practical points of view, the general Neumann boundary problem that rules the pressure p inside an acoustic region Ω when motions are imposed on the boundary $\partial\Omega$. The precise problem consists in finding p such that

$$\nabla^2 p + \frac{\omega^2}{c^2} p = 0 \quad \text{in} \quad \Omega, \quad \frac{\partial p}{\partial n} = D \quad \text{on} \quad \partial\Omega, \tag{94}$$

where ω is the (circular) frequency of vibration; c, the speed of sound; $\partial/\partial n$, the outward normal derivative to the boundary; and where, lastly, $D = -\mathrm{i}\omega\rho V_n$ denotes the given normal quantity of acceleration at the boundary, relative to the imposed normal velocity, V_n, and the mass, ρ, per unit volume of fluid.

Green formulae for the L^2 inner product $\langle\,|\,\rangle$

$$\begin{aligned} \langle \nabla^2 f | g \rangle &= -\langle \nabla f | \nabla g \rangle + \int_{\partial\Omega} \frac{\partial f}{\partial n} g \,\mathrm{d}s, \\ \langle \nabla^2 f | g \rangle - \langle \nabla^2 g | f \rangle &= \int_{\partial\Omega} \frac{\partial f}{\partial n} g \,\mathrm{d}s - \int_{\partial\Omega} \frac{\partial g}{\partial n} f \,\mathrm{d}s \end{aligned} \tag{95}$$

can be invoked to compute the projections, $\langle \psi_m | p \rangle$, of the solution p on the orthonormal family of "rigid cavity" eigenmodes, ψ_m, at eigenfrequencies ω_m, that result from the solution of the homogeneous problem

$$\nabla^2 \psi_m + \frac{\omega_m^2}{c^2} \psi_m = 0 \quad \text{in} \quad \Omega, \quad \frac{\partial \psi_m}{\partial n} = 0 \quad \text{on} \quad \partial\Omega. \tag{96}$$

As a matter of fact, substituting for the boundary values and derivative of p, ψ_m from Eqs. (94), (96) into the second Green formula brings

$$\langle \psi_m | p \rangle = \frac{c^2}{\omega_m^2 - \omega^2} \int_{\partial\Omega} \psi_m D \,\mathrm{d}s. \tag{97}$$

Any attempt to express p as an ordinary superposition $\Sigma \langle \psi_m | p \rangle \psi_m$ will lead however to the same conclusion as in the paper by Kim and Kang, and to the disappointing results that have already been shown in Fig. 2. The boundary velocity equation has, indeed, to be satisfied with a combination of homogeneous modes, each of which has a pointwise zero velocity. The explicit introduction and computation of the orthocomplement will avoid the difficulty and lead to the same general results as before, despite the additional singularity at 0 Hz.

4.2. The method of orthocomplement

(a) *Forward step*: Considering the finite-dimensional vector space, $F = ((\psi_m))_{m=1,\ldots,N}$, spanned by the first N eigenmodes, it seems trivial to write the solution to problem (94) as the sum of its orthogonal projection onto F, plus an orthocomplement, ε_N, orthogonal to F

$$p = \sum_{m=1}^{N} \langle p | \psi_m \rangle \psi_m + \varepsilon_N. \tag{98}$$

From Eqs. (94) and (97) the orthocomplement is seen to satisfy

$$\nabla^2 \varepsilon_N + \frac{\omega^2}{c^2} \varepsilon_N = \sum_{m=1}^{N} \psi_m \left(\int_{\partial\Omega} \psi_m D \,\mathrm{d}s \right) \quad \text{in } \Omega, \quad \frac{\partial \varepsilon_N}{\partial n} = D \quad \text{on} \quad \partial\Omega. \tag{99}$$

The decomposition in two nested sub-problems, A, B, takes here the form

$$\varepsilon_N = \eta_N + \rho_N \left\langle \begin{array}{ll} \nabla^2 \eta_N = \sum_{m=1}^{N} \psi_m \left(\int_{\partial\Omega} \psi_m D \,\mathrm{d}s \right) \quad \text{in } \Omega, & \dfrac{\partial \eta_N}{\partial n} = D \quad \text{on} \quad \partial\Omega \quad \text{(A)} \\ \nabla^2 \rho_N + \dfrac{\omega^2}{c^2} \rho_N = -\dfrac{\omega^2}{c^2} \eta_N \quad \text{in } \Omega, & \dfrac{\partial \rho_N}{\partial n} = 0 \quad \text{on} \quad \partial\Omega \quad \text{(B)} \end{array} \right. \tag{100}$$

It should be easily recognized that (A) is a Laplacian Neumann boundary problem, the solution of which, if there is one, can only be determined within an arbitrary constant. Solvability imposes on the forcing terms to be self-equilibrated, or, so to say, orthogonal to the kernel of the underlying linear operator [32]. The last condition can be written

$$-\int_{\Omega} g_N \,\mathrm{d}v + \int_{\partial\Omega} D \,\mathrm{d}s = 0. \tag{101}$$

It can be suggested to make an explicit use of the 0 Hz constant acoustic normalized eigenmode, $\psi_1 = (\text{meas } \Omega)^{-1/2}$, thereby writing

$$-\int_{\Omega} \psi_1 g_N \,\mathrm{d}v + \int_{\partial\Omega} \psi_1 D \,\mathrm{d}s = 0. \tag{102}$$

Indeed, it can be easily verified that Eq. (102) is fulfilled by D and $g_N = \sum_{m=1}^{N} \psi_m \left(\int_{\partial\Omega} \psi_m D \,\mathrm{d}s\right)$, since

$$\begin{aligned}
&-\int_{\Omega} \psi_1 \sum_{m=1}^{N} \psi_m \left(\int_{\partial\Omega} \psi_m D \,\mathrm{d}s\right) \mathrm{d}v + \int_{\partial\Omega} \psi_1 D \,\mathrm{d}s \\
&= -\sum_{m=1}^{N} \left(\int_{\Omega} \psi_1 \psi_m \mathrm{d}v\right) \left(\int_{\partial\Omega} \psi_m D \,\mathrm{d}s\right) + \int_{\partial\Omega} \psi_1 D \,\mathrm{d}s \\
&= -\sum_{m=1}^{N} \delta_{1m} \left(\int_{\partial\Omega} \psi_m D \,\mathrm{d}s\right) + \int_{\partial\Omega} \psi_1 D \,\mathrm{d}s = 0.
\end{aligned}$$

At the present stage of discussion, the conclusion is thus that problem (A) admits an infinite number of solutions, differing one from the other by an arbitrary constant.

(b) *Coordination step*: Problem (B) being a "smooth" dynamical problem with "continuous" homogeneous boundary conditions, its solution, ρ_N, can be viewed as a strict modal superposition

$$\rho_N = \sum_{k=1}^{\infty} \langle \rho_N | \psi_k \rangle \psi_k. \tag{103}$$

Following the proposed method of orthocomplement, modal projections should be now evaluated in two steps. The first step has been seen to consist in determining the modal projections $\langle \psi_k | \rho_N \rangle$ as functions of the projections $\langle \psi_k | \eta_N \rangle$; actually, substituting for the boundary values and derivatives of ρ_N, ψ_k from Eqs. (103), (96) into the second Green formula gives

$$\langle \rho_N | \psi_k \rangle = \frac{\omega^2}{\omega_k^2 - \omega^2} \langle \eta_N | \psi_k \rangle. \tag{104}$$

The second step is to compute $\langle \eta_N | \psi_k \rangle$; and, indeed, substituting Eqs. (100) and (95) in the second Green formula yields

$$\omega_k^2 \langle \eta_N | \psi_k \rangle = c^2 \left[\int_{\partial\Omega} \psi_k D \,\mathrm{d}s - \sum_{m=1}^{N} \delta_{km} \left(\int_{\partial\Omega} \psi_m D \,\mathrm{d}s \right) \right]. \tag{105}$$

This brings the conclusion that for any $k > 1$

$$\begin{aligned}
\langle \eta_N | \psi_k \rangle &= \frac{c^2}{\omega_k^2} \left[\int_{\partial\Omega} \psi_k D \,\mathrm{d}s - \sum_{m=1}^{N} \delta_{km} \left(\int_{\partial\Omega} \psi_m D \,\mathrm{d}s \right) \right] \\
&= \begin{cases} 0 \quad \text{if} \quad 1 < k \leqslant N, \\ \dfrac{c^2}{\omega_k^2} \int_{\partial\Omega} \psi_k D \,\mathrm{d}s \quad \text{if} \quad N < k. \end{cases}
\end{aligned} \tag{106}$$

The singularity being clearly of order $\sigma = 1$, there is however nothing surprising about the fact that Eq. (105) degenerate to an identity $0 = 0$ when $k = 1$. As in Section 2.2, the indetermination can be eliminated

by setting

$$\langle \eta_N | \psi_1 \rangle = 0. \tag{107}$$

By combining this additional condition and Eqs. (104), (106), it becomes possible to compute all components $\langle \rho_N | \psi_k \rangle$, by means of the formulae

$$\langle \rho_N | \psi_k \rangle = \frac{\omega^2}{\omega_k^2 - \omega^2} \langle \eta_N | \psi_k \rangle = \begin{cases} 0 \quad \text{if} \quad 1 \leqslant k \leqslant N, \\ \dfrac{\omega^2}{\omega_k^2} \dfrac{c^2}{\omega_k^2 - \omega^2} \int_{\partial\Omega} \psi_k D \, \mathrm{d}s \quad \text{if} \quad N < k. \end{cases} \tag{108}$$

On the other hand, by fixing the constant that was left aside in the preliminary discussion, condition (107) fully determines the solution to problem (A), which can be reformulated as

$$\begin{cases} \nabla^2 \eta_N = \sum_{m=1}^{N} \psi_m \left(\int_{\partial\Omega} \psi_m D \, \mathrm{d}s \right) \quad \text{in } \Omega, \quad \dfrac{\partial \eta_N}{\partial n} = D, \\ (\text{meas } \Omega)^{-1/2} \langle \eta_N | \psi_1 \rangle = \int_\Omega \eta_N \, \mathrm{d}v = 0. \end{cases} \tag{109}$$

(c) *Backward step*: As a provisory conclusion, the solution p to the acoustic problem results from the superposition of an ordinary modal sum up to the order N, a pseudo-static term, and an accelerated modal series:

$$p = \left\{ \sum_{m=1}^{N} \psi_k \frac{c^2}{\omega_k^2 - \omega^2} \int_{\partial\Omega} \psi_k D \, \mathrm{d}s \right\} + \eta_N + \left\{ \sum_{m=N+1}^{\infty} \psi_k \frac{\omega^2}{\omega_k^2} \frac{c^2}{\omega_k^2 - \omega^2} \int_{\partial\Omega} \psi_k D \, \mathrm{d}s \right\}, \tag{110}$$

where η_N is the unique solution to (109).

4.3. Finite element solution

For the purpose of numerical analysis, matrices $\mathbf{H}$ and $\mathbf{Q}$, must be classically synthesized, in such a way that

$$\int_\Omega \nabla f \ \nabla g \ \mathrm{d}x = \mathbf{f} \ \mathbf{H} \ \mathbf{g}, \quad \int_\Omega f \ g \ \mathrm{d}x = \mathbf{f} \ \mathbf{Q} \ \mathbf{g}$$

for every pair f, g of functions in $H^1(\Omega)$, approximated by nodal vectors $\mathbf{f}$ and $\mathbf{g}$. Numerical modes and eigenfrequencies can then be defined by solving

$$(\mathbf{H} - \omega_k^2 \mathbf{Q}) \mathbf{\Psi}_k = 0. \tag{111}$$

Assembling the pseudo-static problem is a little less trivial. The first step, as usual, consists in building the associated weak formulation. Namely, the field equation, multiplied by $\delta\eta \in H^1(\Omega)$, must be integrated over the domain and transformed by means of Green's formula to take the boundary condition into account. Solution η_N can thereby be characterized by the variational equality

$$\forall \delta\eta \in H^1(\Omega) \quad : \quad \int_\Omega \nabla(\delta\eta).\nabla\eta_N \, \mathrm{d}v + \int_\Omega \delta\eta g_N \, \mathrm{d}v - \int_{\partial\Omega} \delta\eta D \, \mathrm{d}s = 0, \tag{112}$$

where D is the prescribed boundary data and g_N is defined, as in Eq. (101) by

$$g_N = \sum_{m=1}^{N} \psi_m \left(\int_{\partial\Omega} \psi_m D \, \mathrm{d}s \right).$$

Source vectors $\mathbf{F}$ and $\mathbf{G}_N$, respectively on $\partial\Omega$ and inside Ω, being defined such that

$$\delta\boldsymbol{\eta}^{\mathrm{T}} \mathbf{F} \simeq \int_{\partial\Omega} \delta\eta D \, \mathrm{d}s, \tag{113}$$

$$\delta\boldsymbol{\eta}^{\mathrm{T}} \mathbf{G}_N \simeq \int_\Omega \delta\eta g_N \, \mathrm{d}v, \tag{114}$$

the finite element discretization of Eq. (112) gives the nodal pseudo-static pressure vector $\boldsymbol{\eta}_N$ as the solution to

$$\forall \delta\boldsymbol{\eta} \quad : \quad \delta\boldsymbol{\eta}^{\mathrm{T}}\mathbf{H}\boldsymbol{\eta}_N = \delta\boldsymbol{\eta}^{\mathrm{T}}\mathbf{F} - \delta\boldsymbol{\eta}^{\mathrm{T}}\mathbf{G}_N \tag{115}$$

or, in an equivalent matrix form, to

$$\mathbf{H}\boldsymbol{\eta}_N = \mathbf{F} - \mathbf{G}_N. \tag{116}$$

It now remains to be remarked that the subsidiary orthogonality condition (107) can be written

$$\mathbf{S}^{\mathrm{T}}\mathbf{Q}\boldsymbol{\eta}_N = 0 \tag{117}$$

with a constant vector $\mathbf{S}$ standing for a basis of the subspace of all constant functions.

Using the projector theorem of Appendix B then delivers the definitive expression of the pseudo-inverse solution

$$\boldsymbol{\eta}_N = (1 - \Pi_Q)(\lambda\Pi + \mathbf{H})^{-1}(\mathbf{F} - \mathbf{G}_N) \quad \text{for any } \lambda \neq 0.$$

It can be noted that $\Pi = \mathbf{S}(\mathbf{S}^t\mathbf{S})^{-1}\mathbf{S}^t$ is the full constant matrix

$$\Pi = \frac{1}{\overline{N}}\begin{bmatrix} 1 & 1 & 1 \\ 1 & 1 & 1 \\ & & \\ 1 & 1 & 1 \end{bmatrix}, \tag{118}$$

where $\overline{N}$ is the total number of nodes. It should be observed, in addition, that this operator is ill-conditioned for small values of λ since $\lambda\Pi + \mathbf{H} \simeq \mathbf{H}$, as well as for large values, since, in that case, $\lambda\Pi + \mathbf{H} \simeq \lambda\Pi$. The use of intermediate values of λ, of the order of magnitude $\overline{N}\|H\|$, is thus highly recommended.

4.4. Numerical example of a 2D cavity

The preceding formulae have been tested in a 2D-cavity filled with air, at the standard 20 °C temperature, that is to say, with speed of sound $c = 340\,\mathrm{m/s}$ and mass density $\rho = 1.2\,\mathrm{kg/m^3}$. The cavity is a $0.7\,\mathrm{m} \times 0.3\,\mathrm{m}$ rectangle; as indicated on Fig. 14 a unit acceleration is imposed on a small segment Ls, at the boundary of the cavity.

The 10 first eigenfrequencies are given in Table 4.

Fig. 15 shows the acoustic pressures and velocities obtained by ordinary modal summation, direct computation, and hybrid spectral formulae.

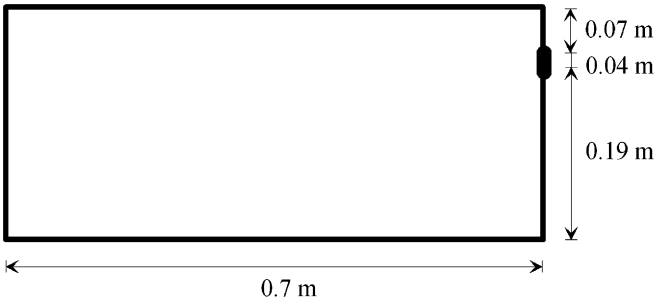

Fig. 14. 2D acoustic cavity.

Table 4
Eigenfrequencies of the acoustic cavity

Mode number	1	2	3	4	5	6	7	8	9	10
Frequency (Hz)	0	242.9	486.2	567.2	617	730.3	747	924.6	975.4	1128

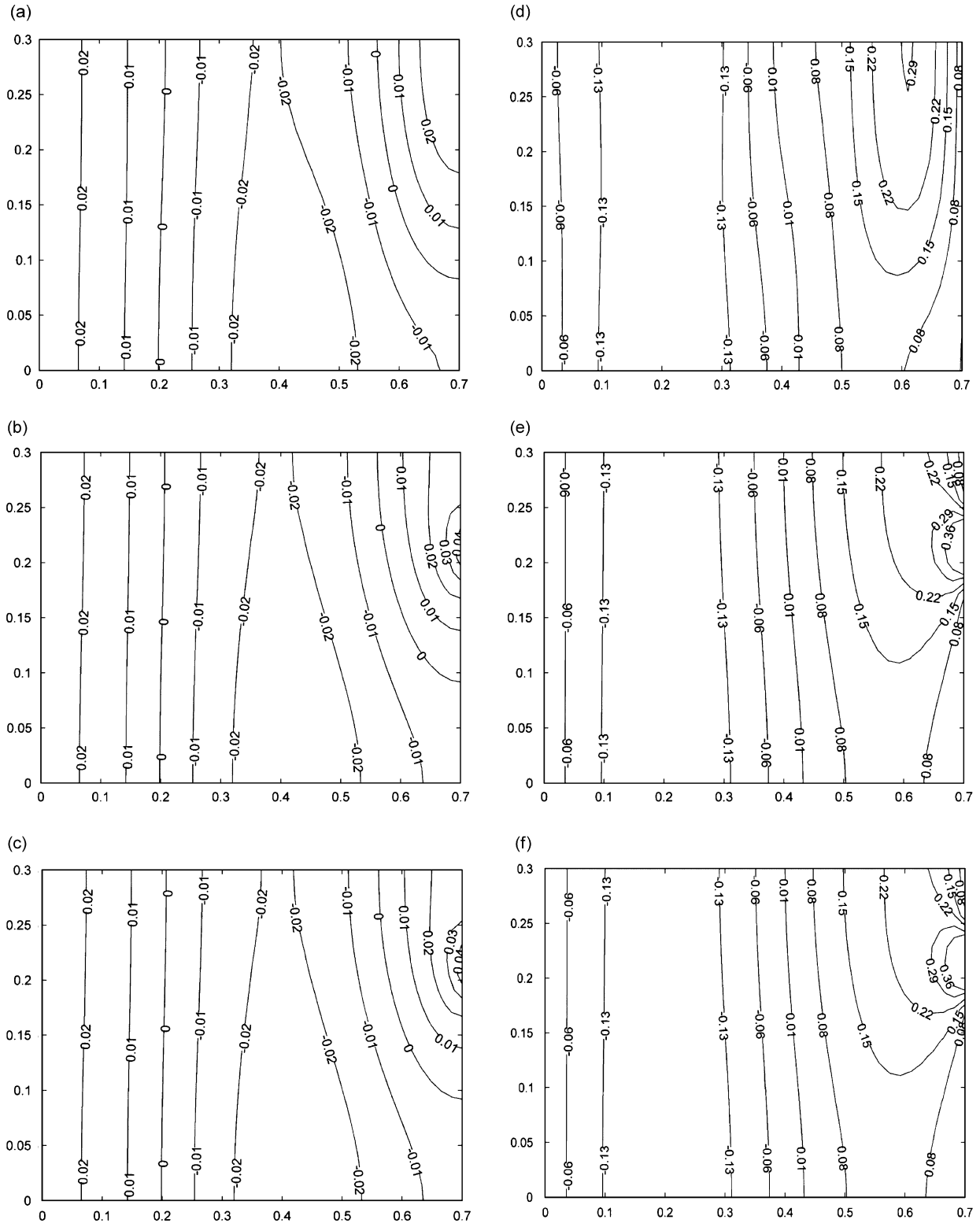

Fig. 15. Acoustic pressure in the 2D acoustic cavity: (a) ordinary modal sum; (b) hybrid modal sum; (c) direct computation. Acoustic velocity: (d) ordinary modal sum; (e) hybrid modal sum; (f) direct computation.

The minimal hybrid formula of order $N = 1$,

$$p = -\frac{c^2}{\omega^2}\frac{1}{\text{meas}(\Omega)}\int_{\partial\Omega} D\,\mathrm{d}s + \eta_1 + \left\{\sum_{m=2}^{\infty}\psi_m\frac{\omega^2}{\omega_m^2}\frac{c^2}{\omega_m^2-\omega^2}\int_{\partial\Omega}\psi_m D\,\mathrm{d}s\right\} \tag{119}$$

with

$$\begin{cases} \nabla^2\eta_1 = \dfrac{1}{\text{meas}(\Omega)}\int_{\partial\Omega} D\,\mathrm{d}s \quad \text{in } \Omega, \quad \dfrac{\partial\eta_1}{\partial n} = D, \\ \int_\Omega \eta_1\,\mathrm{d}v = 0 \end{cases} \tag{120}$$

is of special interest and will be the object of a future standard development.

5. Conclusion

The above computation of the acoustic receptance at the boundary of a cavity has been used to place and design Helmholtz resonators inside automotive cells. A precise account of the coupling technique that mixes together numerical and analytical computations will be given in a forthcoming paper.

The proposed technique can also address mechanical systems of a greater complexity than resonators. By a repeated use of the proposed method, it seems indeed possible to assemble the acoustic impedances that determine the coupled vibro-acoustic field. This approach would fill a gap between modal analysis and acoustics, and first examples are presently under study.

Beyond coupling applications, a connection can be made with much more general problems of modal synthesis. Indeed, the various kinds of operations that constitute the pyramid of modal methods can be summarized as follows:

(a) receptance synthesis aims to equip subsystems of correct receptance relations, which is perfectly suited for experimental or design applications involving a low number of conception parameters;
(b) with increasing dimension of matrices, the preceding approach, that involves frequency dependent full matrices, and relatively complex rules of assembly, becomes quite ineffective and one must pose problems

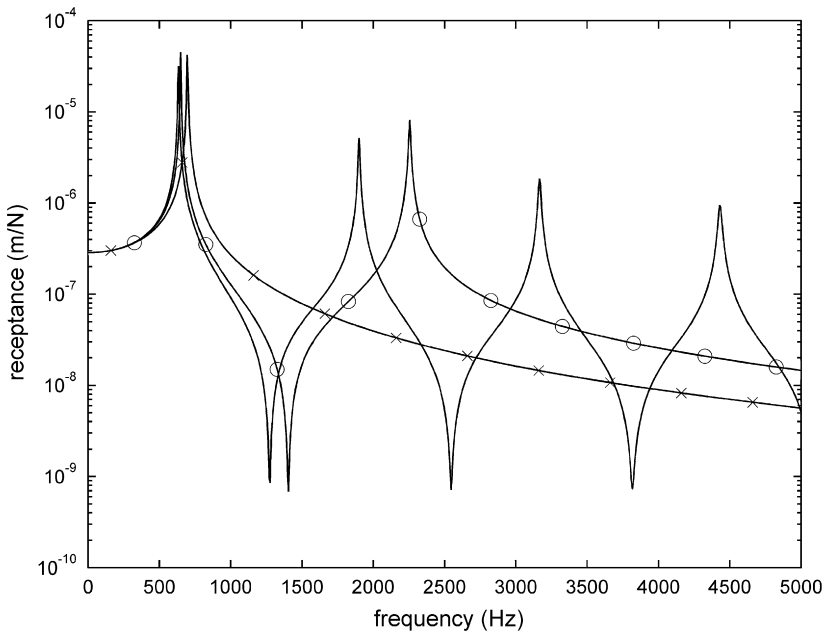

Fig. 16. Receptance at the free end of the fixed–free chain: —— exact; × 1 mass equivalent oscillator; ○ 2 mass equivalent oscillator.

of "model reduction", which consist in finding constant mass or rigidity operators that approximately describes the behaviour of subsystems;

(c) lastly, assembling the local mass and stiffness operators to describe the behaviour of a global structure, too complex to be analysed as a whole, is the proper task of modal synthesis.

The paper concentrated on level (a) and maybe some readers have wondered why many quotations in the bibliography are in fact relevant to levels (b) and (c). The explanation is in the following.

The dynamic stiffness of a subsystem 1, is given by

$$\mathbf{f}_1 = \left\{(\mathbf{K}_{11} - \mathbf{M}_{11}\omega^2) - (\mathbf{K}_{12} - \mathbf{M}_{12}\omega^2)(\mathbf{K}_{22} - \mathbf{M}_{22}\omega^2)^{-1}(\mathbf{K}_{21} - \mathbf{M}_{21}\omega^2)\right\}\mathbf{x}_1 \tag{121}$$

provided the complementary part, 2, is free of external efforts.

The problem of model reduction consists in finding $\mathbf{K}_1$ and $\mathbf{M}_1$ such that

$$\mathbf{f}_1 \simeq (\mathbf{K}_1 - \mathbf{M}_1\omega^2)\mathbf{x}_1. \tag{122}$$

In this new context, the formulae that have been developed in the present paper can be read, and used, as general algebraic expressions of inverse matrices. Let it be supposed that in the considered example, the complementary part, 2, is at rest on a given support. The global stiffness matrix $\mathbf{K}$ is then invertible and one can use Eq. (21) to write the approximate identity

$$(\mathbf{K}_1 - \mathbf{M}_1\omega^2)\left\{\mathbf{\Phi}_1[\mathbf{D}(\omega) - \mathbf{D}(0)]\mathbf{\Phi}_1^{\mathrm{T}} + \mathbf{P}_1\mathbf{K}^{-1}\mathbf{P}_1^{\mathrm{T}}\right\} - \mathbf{1} \simeq \mathbf{0}. \tag{123}$$

A Taylor expansion with respect to ω^2 leads to the best low-frequency approximations

$$\mathbf{K}_1 = (\mathbf{P}_1\mathbf{K}^{-1}\mathbf{P}_1^{\mathrm{T}})^{-1}, \tag{124}$$

$$\mathbf{M}_1 = (\mathbf{P}_1\mathbf{K}^{-1}\mathbf{P}_1^{\mathrm{T}})^{-1}\Phi_1\Omega^{-2}\Omega^{-2}\Phi_1^{\mathrm{T}}(\mathbf{P}_1\mathbf{K}^{-1}\mathbf{P}_1^{\mathrm{T}})^{-1}. \tag{125}$$

The receptances that can be computed at the end of the 100-mass chain of Section 2 after reduction to a single oscillator or a more complex 2-mass oscillator are drawn in Fig. 16. Only 20 modes have been used to write Eqs. (124) and (125). Other techniques are presently under study, and especially the spectral inversion of $(\mathbf{K}_{22} - \mathbf{M}_{22}\omega^2)$ in Eq. (121), that leads to revisit fixed-interface computations [22]. Clearly there is still quite a way to go, but Eqs. (124) and (125) are interesting examples of model reduction formulae with static modes.

Acknowledgements

The authors are particularly indebted to Dr. Olivier Sauvage, for very helpful advice, comments and discussions, and last but not least, for his decisive contribution to the construction of the bibliography.

They address quite special acknowledgements to Mr. Philippe Cuvelier, Head of the VA Laboratory of Vibration and Acoustics in the Research Department of ESTACA, for his constant moral and material help.

Appendix A. Elementary Moore–Penrose pseudo-inverses for rectangular systems of maximum rank

This annex is devoted to the pseudo-inverse operations that are required to deal with the 0 Hz-singularity of stiffness matrices of floating systems. Its reading only requires some acquaintance with the basic notions of linear algebra like image, kernel, and transposition. A frequent use will be made of the elementary lemma that stipulates that in usual orthogonal coordinates

$$(\mathrm{Ker}\ \mathbf{S})^{\perp} = \mathrm{Im}\ \mathbf{S}^{\mathrm{T}}. \tag{A.1}$$

This will be referred to as Lagrange lemma, since it constitutes the very basis of virtual work methods [33].

One will consider here systems in the form

$$\mathbf{S}\mathbf{x} = \mathbf{f} \tag{A.2}$$

with $\mathbf{S}$ a rectangular (p,q)-matrix, $p \neq q$, satisfying the maximum rank condition

$$\mathrm{rank}(\mathbf{S}) = \min(p, q). \tag{A.3}$$

Such systems cannot be solved in an ordinary sense since they either suffer from overdetermination when $p>q$ or from indetermination when $p<q$. Least-squares techniques can then either be used to deliver approximate solutions or to make a choice among an infinity of solutions. The associated matrices are known as Moore–Penrose pseudo-inverses since it was recognized that they satisfied the full axiomatic set that had been earlier devised by the two authors for the abstract definition of pseudo-inverses.

(a) *Overdeterminated systems*: The number p of equations being greater than the number q of unknowns, one cannot find any solution to the inversion problem. The difficulty can be lifted by replacing the strict equality (A.2) by the minimization of the distance from $\mathbf{Sx}$ to $\mathbf{f}$:

$$\text{Find } \mathbf{x}^* \text{ that minimizes } F(\mathbf{x}) = \tfrac{1}{2}\|\mathbf{Sx}-\mathbf{f}\|^2.$$

For the usual Euclidian norm, function F and its first variation δF have the following expressions:

$$F(\mathbf{x}) = \tfrac{1}{2}\mathbf{x}^{\mathrm{T}}\mathbf{S}^{\mathrm{T}}\mathbf{Sx} - \tfrac{1}{2}(\mathbf{x}^{\mathrm{T}}\mathbf{S}^{\mathrm{T}}\mathbf{f}+\mathbf{f}^{\mathrm{T}}\mathbf{Sx}) + \tfrac{1}{2}\mathbf{f}^{\mathrm{T}}\mathbf{f} = \tfrac{1}{2}\langle \mathbf{S}^{\mathrm{T}}\mathbf{Sx}|\mathbf{x}\rangle - \langle \mathbf{S}^{\mathrm{T}}\mathbf{f}|\mathbf{x}\rangle + \tfrac{1}{2}\mathbf{f}^{\mathrm{T}}\mathbf{f} \tag{A.4}$$

$$\delta F(\mathbf{x}) = \tfrac{1}{2}\langle \mathbf{S}^{\mathrm{T}}\mathbf{S}\delta\mathbf{x}|\mathbf{x}\rangle + \tfrac{1}{2}\langle \mathbf{S}^{\mathrm{T}}\mathbf{Sx}|\delta\mathbf{x}\rangle - \langle \mathbf{S}^{\mathrm{T}}\mathbf{f}|\delta\mathbf{x}\rangle = \langle \mathbf{S}^{\mathrm{T}}\mathbf{Sx}-\mathbf{S}^{\mathrm{T}}\mathbf{f}|\delta\mathbf{x}\rangle \tag{A.5}$$

where $<>$ stands for the Euclidian inner product.

Matrix $\mathbf{S}$ is constituted by q columns of p terms, $p>q$. These columns are linearly independent thanks to the maximum rank hypothesis. Consequently, the matrix $\mathbf{S}^{\mathrm{T}}\mathbf{S}$ in the expression of δF, is invertible. As a matter of fact, every element $\boldsymbol{\alpha}$ of its kernel is shown to be zero by the following chain of implications:

$$\mathbf{S}^{\mathrm{T}}\mathbf{S}\alpha = \mathbf{0} \Rightarrow \alpha^{\mathrm{T}}\mathbf{S}^{\mathrm{T}}\mathbf{S}\alpha = \mathbf{0} \Rightarrow \langle \mathbf{S}\alpha|\mathbf{S}\alpha\rangle = \mathbf{0} \Rightarrow \mathbf{S}\alpha = \mathbf{0} \Rightarrow \boldsymbol{\alpha} = \mathbf{0}.$$

The stationnarity condition $\delta F(\mathbf{x}^*) = 0$ for every $\delta\mathbf{x}$, then brings the expression of the Moore–Penrose pseudo-inverse

$$\mathbf{x}^* = (\mathbf{S}^{\mathrm{T}}\mathbf{S})^{-1}\mathbf{S}^{\mathrm{T}}\mathbf{f}. \tag{A.6}$$

The vector $\mathbf{Sx}^*$ is the element of Im $\mathbf{S}$ which lies at the shortest distance of the given $\mathbf{f}$. The orthogonal projector on the subspace generated by the columns of $\mathbf{S}$, is thus given by

$$\boldsymbol{\Pi} = \mathbf{S}(\mathbf{S}^{\mathrm{T}}\mathbf{S})^{-1}\mathbf{S}^{\mathrm{T}}. \tag{A.7}$$

One can also consider any positive definite symmetric matrix $\mathbf{M}$ and decide to minimize the M-distance instead of the Euclidian distance

$$\begin{aligned} G(\mathbf{x}) &= \tfrac{1}{2}(\mathbf{Sx}-\mathbf{f})^{\mathrm{T}}\mathbf{M}(\mathbf{Sx}-\mathbf{f}) = \tfrac{1}{2}\mathbf{x}^{\mathrm{T}}\mathbf{S}^{\mathrm{T}}\mathbf{MSx} - \tfrac{1}{2}\left(\mathbf{x}^{\mathrm{T}}\mathbf{S}^{\mathrm{T}}\mathbf{Mf}+\mathbf{f}^{\mathrm{T}}\mathbf{MSx}\right) + \tfrac{1}{2}\mathbf{f}^{\mathrm{T}}\mathbf{Mf} \\ &= \tfrac{1}{2}\langle \mathbf{S}^{\mathrm{T}}\mathbf{MSx}|\mathbf{x}\rangle - \langle \mathbf{S}^{\mathrm{T}}\mathbf{Mf}|\mathbf{x}\rangle + \tfrac{1}{2}\mathbf{f}^{\mathrm{T}}\mathbf{Mf} \end{aligned}$$

The first variation δG can now be formulated as

$$\delta G(\mathbf{x}) = \langle \mathbf{S}^{\mathrm{T}}\mathbf{MSx}-\mathbf{S}^{\mathrm{T}}\mathbf{Mf}|\delta\mathbf{x}\rangle. \tag{A.8}$$

This leads to the following general expressions of pseudo-inverses and projectors

$$\mathbf{x}^{*\mathbf{M}} = (\mathbf{S}^{\mathrm{T}}\mathbf{MS})^{-1}\mathbf{S}^{\mathrm{T}}\mathbf{Mf}, \tag{A.9}$$

$$\boldsymbol{\Pi}^{\mathbf{M}} = \mathbf{S}(\mathbf{S}^{\mathrm{T}}\mathbf{MS})^{-1}\mathbf{S}^{\mathrm{T}}\mathbf{M}. \tag{A.10}$$

(b) *Underdeterminated systems*: The number p of equations is now smaller than the number q of unknowns. The p equations are linearly independent, by the maximum rank hypothesis. System (A.2) then admits an infinity of solutions. The minimization of an appropriate norm permits the computation of distinguished solutions to the considered system. The choice of the Euclidian norm, for instance, will lead to the discussion and solution to

$$\text{Find } \mathbf{x}^* \text{ that minimizes } H(\mathbf{x}) = \tfrac{1}{2}\|\mathbf{x}\|^2, \text{ subject to } \mathbf{Sx}-\mathbf{f}.$$

Function H and its first variation δH can be expressed as

$$H(\mathbf{x}) = \tfrac{1}{2}\mathbf{x}^{\mathrm{T}}\mathbf{x}, \quad \delta H(\mathbf{x}) = \mathbf{x}^{\mathrm{T}}\delta\mathbf{x} = \langle \mathbf{x}|\delta\mathbf{x}\rangle. \tag{A.11}$$

At the optimum, every admissible $\delta\mathbf{x}$- that is to say every $\delta\mathbf{x}$ satisfying, $\mathbf{S}\,\delta\mathbf{x} = 0$ or, in other words, every element of Ker $\mathbf{S}$—cannot alter the first variation $\delta H(\mathbf{x}^*) = \langle \mathbf{x}^*, \delta\mathbf{x}\rangle$ and thus must be orthogonal to $\mathbf{x}^*$. The optimum $\mathbf{x}^*$ therefore belongs to the orthogonal of Ker $\mathbf{S}$ which, by Lagrange lemma, is also the image of $\mathbf{S}^{\mathrm{T}}$. There thus exists some $\Lambda \in R^p$, such that

$$\mathbf{x}^* = \mathbf{S}^{\mathrm{T}}\boldsymbol{\Lambda}. \tag{A.12}$$

This new vector is known as the vector of Lagrange's multipliers. It satisfies, because of the initial equation

$$\mathbf{S}\mathbf{S}^{\mathrm{T}}\boldsymbol{\Lambda} = \mathbf{f}. \tag{A.13}$$

The operator $\mathbf{S}\,\mathbf{S}^{\mathrm{T}}$ is invertible, by a direct transposition of the argumentation about the term $\mathbf{S}^{\mathrm{T}}\,\mathbf{S}$ in the previous paragraph. In this way, one finds the following expression of $\mathbf{x}^*$:

$$\mathbf{x}^* = \mathbf{S}^{\mathrm{T}}(\mathbf{S}^{\mathrm{T}}\mathbf{S})^{-1}\mathbf{f}. \tag{A.14}$$

The general solution to the initial system is therefore

$$\mathbf{x} = \mathbf{S}^{\mathrm{T}}(\mathbf{S}\mathbf{S}^{\mathrm{T}})^{-1}\mathbf{f} + \mathbf{S}\boldsymbol{\alpha}, \tag{A.15}$$

with an arbitrary $\boldsymbol{\alpha} \in R^p$.

As in the preceding paragraph, any non-Euclidian metric, based on a symmetric positive definite matrix $\mathbf{M}$, can be substituted to the ordinary Euclidian metric. Problem (A.11) turns to

$$\text{Find } \mathbf{x}^M \text{ that minimizes } J(\mathbf{x}) = \tfrac{1}{2}\|\mathbf{x}\|_M^2 = \tfrac{1}{2}\mathbf{x}^{\mathrm{T}}\mathbf{M}\mathbf{x} \text{ subject to } \mathbf{S}\mathbf{x} - \mathbf{f}.$$

The first variation can now be written as

$$\delta J(\mathbf{x}) = \mathbf{x}^{\mathrm{T}}\mathbf{M}\delta\mathbf{x} + \delta\mathbf{x}^{\mathrm{T}}\mathbf{M}\mathbf{x} = \langle \mathbf{M}\mathbf{x}|\delta\mathbf{x}\rangle. \tag{A.16}$$

The condition of stationnarity at $\mathbf{x}^M$ now stipulates that $\mathbf{M}\,\mathbf{x}^M$ is orthogonal to Ker $\mathbf{S}$ and thus belongs to $\mathrm{Im}\,\mathbf{S}^{\mathrm{T}}$. One can introduce a vector of Lagrange multipliers such that

$$\mathbf{M}\mathbf{x}^{\mathrm{M}} = \mathbf{S}^{\mathrm{T}}\boldsymbol{\Lambda} \tag{A.17}$$

and finally write the pseudo-inverse solution as

$$\mathbf{x}^M = \mathbf{M}^{-1}\mathbf{S}^{\mathrm{T}}(\mathbf{S}\mathbf{M}^{-1}\mathbf{S}^{\mathrm{T}})^{-1}\mathbf{f}. \tag{A.18}$$

Appendix B. Special techniques of pseudo-inversion for square singular stiffness matrices; the projector theorems

Pseudo-inverse and projector formulae of Appendix A permits the solution of singular systems associated with a square symmetric singular matrix $\mathbf{K}$ when a spanning matrix $\mathbf{S}$ of the kernel of $\mathbf{K}$ is occasionally at disposal. Studying that case is really worthwhile, because the kernel of every mechanical floating stiffness matrix reduces to a set of known rigid motions. Although the considered matrices are not of maximum rank, a considerable amount of computations can be spared by an adequate use of the proposed formulae.

Indeed, let

$$\mathbf{K}\mathbf{x} = \mathbf{f}. \tag{B.1}$$

be a system of the preceding type, with $\mathbf{K} = \mathbf{K}^{\mathrm{T}}$, $\det(\mathbf{K}) = 0$ and $\mathbf{S}$, a $p \times q$ matrix of minimum rank, such that

$$\mathrm{Ker}(\mathbf{K}) = \mathrm{Im}(\mathbf{S}) = \left\{\mathbf{y} \in R^p | \exists \boldsymbol{\beta} \in R^q : \mathbf{y} = \mathbf{S}\boldsymbol{\beta}\right\}. \tag{B.2}$$

System (B.1) is soluble iff $\mathbf{f}$ belongs to the image of $\mathbf{K}$, or by Lagrange's lemma is orthogonal to Ker($\mathbf{K}$), or in other words, iff it satisfies the integrability condition:

$$\mathbf{S}^{\mathrm{T}}\mathbf{f} = 0. \tag{B.3}$$

In this case, the solution is not unique. It is usually written, by a mere argument of linearity, as

$$\mathbf{x} = \mathbf{x}_0 + \mathbf{S}\boldsymbol{\alpha} \tag{B.4}$$

with $\mathbf{x}_0$ a distinguished solution and $\mathbf{S}\boldsymbol{\alpha}$, $\boldsymbol{\alpha}$ in R^q, an arbitrary element of Ker($\mathbf{K}$).

The point is to produce additional conditions or relations-say $\mathbf{Ax} = 0$-that could constrain the initial system to deliver a well-posed problem

$$\begin{cases} \mathbf{Kx} = \mathbf{f}, \\ \mathbf{Ax} = \mathbf{0}, \end{cases} \tag{B.5}$$

whose unique solution, once computed, could be taken as the special solution $\mathbf{x}_0$. Matrix $\mathbf{K}$ is a $p \times p$ matrix with rank $p-q$, since q, by (B.2), is the dimension of Ker($\mathbf{K}$). Additional restrictions should thus bring q independent relations compatible with system (B.1). Given an arbitrary positive definite matrix $\mathbf{M}$, a very simple choice consists in imposing on the solution to be M-orthogonal to Ker($\mathbf{K}$). This does not only bring the correct number of equations but also ensures compatibility and uniqueness. Indeed, the corresponding $\mathbf{x}_0$, or say $\mathbf{x}_M$, is the only point of intersection of the set of solutions with a complementary M-orthogonal subspace.

Two theorems are now proposed, which can be of a great help in effective mechanical computations: Theorem 1 for the canonical metric $\mathbf{M} = \mathbf{1}$; Theorem 2, as a corollary, for an arbitrary metric $\mathbf{M}$.

(a) Theorem 1. *As far as* $\mathbf{f}$ *obeys the integrability condition, the singular square system admits the general solution*:

$$\mathbf{x} = (\lambda\mathbf{\Pi} + \mathbf{K})^{-1}\mathbf{f} + \mathbf{S}\boldsymbol{\alpha}, \tag{B.6}$$

where λ *is a totally arbitrary non-zero number;* $\boldsymbol{\alpha}$, *a totally arbitrary vector in* R^q; *and,* $\mathbf{\Pi} = \mathbf{S}(\mathbf{S}^{\mathrm{T}}\mathbf{S})^{-1}\mathbf{S}^{\mathrm{T}}$, *the orthogonal projector on the kernel of* $\mathbf{K}$. *The distinguished solution*

$$\mathbf{x}^* = (\lambda\mathbf{\Pi} + \mathbf{K})^{-1}\mathbf{f} \tag{B.7}$$

is totally independent of λ *and can be identified to the unique element of* Im($\mathbf{K}$) *that satisfies* $\mathbf{Kx} = \mathbf{f}$. *It corresponds to the SVD inverse of the symmetric matrix* $\mathbf{K}$, *or, by Lagrange lemma, to the only vector that satisfies both* $\mathbf{Kx} = \mathbf{f}$ and $\mathbf{S}^{\mathrm{T}}\mathbf{x} = \mathbf{0}$.

For each $\lambda \neq 0$, $\lambda\mathbf{\Pi} + \mathbf{K}$ is invertible. Indeed, Ker($\mathbf{K}$) and Im($\mathbf{K}$) form a pair of complementary subspaces,

$$R^q = \mathrm{Im}(\mathbf{K}) \oplus \mathrm{Ker}(\mathbf{K}) \tag{B.8}$$

along which any vector can be decomposed in a unique manner. Because $\lambda\mathbf{\Pi z} \in \mathrm{Ker}(\mathbf{K})$, and $\mathbf{Kz} \in \mathrm{Im}(\mathbf{K})$, any vector $\mathbf{z}$ satisfying

$$(\lambda\mathbf{\Pi} + \mathbf{K})\mathbf{z} = \mathbf{0} \tag{B.9}$$

(with $\lambda \neq 0$) is necessarily such that

$$\mathbf{\Pi z} = \mathbf{0} \quad \text{and} \quad \mathbf{Kz} = \mathbf{0}.$$

This implies $\mathbf{z} = 0$, since the considered vector simultaneously belongs to the two complementary subspaces. The operator, whose kernel reduces itself to zero is invertible.

As a consequence, there exists some $\mathbf{x}^*$ that verifies

$$\mathbf{x}^* = (\lambda\mathbf{\Pi} + \mathbf{K})^{-1}\mathbf{f} \tag{B.10}$$

or, equivalently,

$$\lambda\mathbf{\Pi x}^* + \mathbf{Kx}^* = \mathbf{f}.$$

The vector $\mathbf{Kx}^*$ is an element of Im($\mathbf{K}$). This is also valid for $\mathbf{f}$, which is supposed to satisfy the integrability condition. On the other hand, $\lambda\mathbf{\Pi x}^*$ is an element of Ker($\mathbf{K}$). Using the same argument as before, one has necessarily the two separate conditions

$$\mathbf{Kx}^* = \mathbf{f}, \quad \mathbf{\Pi x}^* = 0.$$

The conclusion is, first, that $\mathbf{x}^*$ is a solution to the considered system, and, second, that it lies in the image, Im($\mathbf{K}$).

Finally, uniqueness and independence with respect to λ result from the fact that two solutions $\mathbf{x}_1$, $\mathbf{x}_2$ that belong to Im(K) necessarily coincide, since their difference must simultaneously satisfy

$$\mathbf{x}_1 - \mathbf{x}_2 \in \mathrm{Im}(\mathbf{K}), \quad \mathbf{x}_1 - \mathbf{x}_2 \in \mathrm{Ker}(\mathbf{K}).$$

(b) Theorem 2. *When f satisfies the integrability condition, the singular square system admits the general solution:*

$$\mathbf{x} = (\mathbf{1} - \mathbf{\Pi}^M)(\lambda\mathbf{\Pi} + \mathbf{K})^{-1}\mathbf{f} + \mathbf{S}\boldsymbol{\alpha}, \tag{B.11}$$

where λ is a totally arbitrary non-zero number; $\boldsymbol{\alpha}$, a totally arbitrary vector in R^q; and where $\mathbf{\Pi} = \mathbf{S}(\mathbf{S}^{\mathrm{T}}\mathbf{S})^{-1}\mathbf{S}^{\mathrm{T}}$ and $\mathbf{\Pi}^M = \mathbf{S}(\mathbf{S}^{\mathrm{T}}\mathbf{M}\mathbf{S})^{-1}\mathbf{S}^{\mathrm{T}}\mathbf{M}$ are the orthogonal projectors on the kernel of $\mathbf{K}$, respectively for the Euclidian metric and the M-orthogonal one.

The distinguished solution

$$\mathbf{x}^M = (\mathbf{1} - \mathbf{\Pi}^M)(\lambda\mathbf{\Pi} + \mathbf{K})^{-1}\mathbf{f} \tag{B.12}$$

is the unique element M-orthogonal to Ker(K) *that satisfies $\mathbf{K}\mathbf{x} = \mathbf{f}$, or equivalently, the only vector that satisfies both $\mathbf{K}\mathbf{x} = \mathbf{f}$* and *$\mathbf{S}^{\mathrm{T}}\mathbf{M}\mathbf{x} = \mathbf{0}$. This last conditions define a unique linear peudo-inverse operator $\mathbf{K}^{\dagger[M]}$ whose expression is given by Eq.* (B.12).

The point is clearly to exhibit a solution $\mathbf{x}^M$ satisfying $\mathbf{S}^{\mathrm{T}}\mathbf{M}\mathbf{x}^M$. By Theorem 1, such an $\mathbf{x}^M$ can be searched for under the form

$$\mathbf{x}^M = \mathbf{x}^* + \mathbf{S}\boldsymbol{\beta} \tag{B.13}$$

with an unknown vector $\boldsymbol{\beta}$ satisfying the orthogonality condition

$$\mathbf{S}^{\mathrm{T}}\mathbf{M}\mathbf{x}^* + \mathbf{S}^{\mathrm{T}}\mathbf{M}\mathbf{S}\boldsymbol{\beta} = \mathbf{0}. \tag{B.14}$$

One finds in that way

$$\mathbf{x}^M = \left[\mathbf{1} - \mathbf{S}(\mathbf{S}^{\mathrm{T}}\mathbf{M}\mathbf{S})^{-1}\mathbf{S}^{\mathrm{T}}\mathbf{M}\right]\mathbf{x}^* \tag{B.15}$$

with the expression (A.10) of the M-projector on the right-hand side of the formula.

Appendix C. Laurent expansion of the dynamic response at 0 Hz

Laurent or Taylor expansions of frequency response functions are of a great help in theoretical developments. Taylor formulae for fixed systems can be found, for example, in Ref. [19]. The present appendix only addresses the singular case of a floating system with σ rigid modes.

Starting from the algebraic identity

$$\frac{1}{\omega_m^2 - \omega^2} = \frac{1}{\omega_m^2}\left(1 - \frac{\omega^2}{\omega_m^2}\right)^{-1} = \frac{1}{\omega_m^2}\left(1 + \frac{\omega^2}{\omega_m^2} + \frac{\omega^4}{\omega_m^4} + \cdots + \frac{\omega^{2k}}{\omega_m^{2k}} + \cdots\right) \tag{C.1}$$

any ordinary spectral sum can take the form of a Laurent expansion at origin:

$$\mathbf{x}(\omega) = -\frac{1}{\omega^2}\mathbf{x}_0 + \mathbf{x}_1 + \omega^2\mathbf{x}_2 + \omega^4\mathbf{x}_3 + \cdots + \omega^{2k-2}\mathbf{x}_k + \cdots. \tag{C.2}$$

The successive coefficients are given by

$$\mathbf{x}_0 = \sum_{m=1}^{\sigma} \mathbf{\Psi}_m\mathbf{\Psi}_m^{\mathrm{T}}\mathbf{f}, \ldots, \quad \mathbf{x}_k = \sum_{m=\sigma+1}^{\overline{N}} \frac{\mathbf{\Psi}_m\mathbf{\Psi}_m^{\mathrm{T}}}{\omega_m^{2k}}\mathbf{f} \quad (1 \leqslant k \leqslant \overline{N} - 1). \tag{C.3}$$

Putting down the Laurent expansion inside the basic equation of motion yields a cascade of identification relations that are of great interest in the interpretation of the 0 Hz modal contribution

$$\begin{aligned} &\mathbf{K}\mathbf{x}_0 = \mathbf{0} \quad \rightarrow \quad \mathbf{K}\mathbf{x}_1 + \mathbf{M}\mathbf{x}_0 = \mathbf{f} \quad \rightarrow \quad \mathbf{K}\mathbf{x}_2 \\ &-\mathbf{M}\mathbf{x}_1 = \mathbf{0} \quad \rightarrow \cdots \rightarrow \quad \mathbf{K}\mathbf{x}_k - \mathbf{M}\mathbf{x}_{k-1} = \mathbf{0} \quad \rightarrow \cdots \end{aligned} \tag{C.4}$$

(a) *Coefficient* $\mathbf{x}_0$: The first equation in Eq. (C.4) means that $\mathbf{x}_0$ is a rigid motion. If $\mathbf{S}$ denotes the spanning matrix of the set of such displacements, one may write

$$\mathbf{K}\mathbf{x}_0 = 0 \Rightarrow \mathbf{x}_0 \in \mathrm{Ker}\mathbf{K} \Rightarrow \exists \boldsymbol{\gamma} : \quad \mathbf{x}_0 = \mathbf{S}\boldsymbol{\gamma}. \tag{C.5}$$

Looking carefully at the second equation then brings the following implications:

$$\mathbf{K}\mathbf{x}_1 + \mathbf{M}\mathbf{x}_0 = \mathbf{f} \Rightarrow (\mathbf{M}\mathbf{x}_0 - \mathbf{f}) \in \mathrm{Im}\mathbf{K} \Rightarrow \mathbf{S}^{\mathrm{T}}(\mathbf{M}\mathbf{x}_0 - \mathbf{f}) = 0. \tag{C.6}$$

As a direct consequence of the two right-hand relations, one now observes that the unknown vector γ satisfies

$$\mathbf{S}^{\mathrm{T}}\mathbf{M}\mathbf{S}\boldsymbol{\gamma} = \mathbf{S}^{\mathrm{T}}\mathbf{f}, \tag{C.7}$$

which finally yields

$$\mathbf{x}_0 = \mathbf{S}(\mathbf{S}^{\mathrm{T}}\mathbf{M}\mathbf{S})^{-1}\mathbf{S}^{\mathrm{T}}\mathbf{f}. \tag{C.8}$$

In the most common case when $\sigma = 6$, this last formula can be easily interpreted in terms of rigid body accelerations:

$\mathbf{S}^{\mathrm{T}}\mathbf{f} \in R^6$ is the vector of resultants and moments corresponding to the given forces $\mathbf{f}$;
$\mathbf{S}^{\mathrm{T}}\mathbf{M}\mathbf{S}$ is the condensed 6×6 mass matrix that rules rigid motions;
$\mathbf{y} = (\mathbf{S}^{\mathrm{T}}\mathbf{M}\mathbf{S})^{-1}\mathbf{S}^{\mathrm{T}}\mathbf{f} \in R^6$ gives the six intrinsic components of the rigid acceleration;
$\mathbf{S}\mathbf{y} = \mathbf{S}(\mathbf{S}^{\mathrm{T}}\mathbf{M}\mathbf{S})^{-1}\mathbf{S}^{\mathrm{T}}\mathbf{f}$, finally, is the expression on the physical degrees of freedom of the rigid body acceleration field.

One gets, by identification with the first of Eq. (C.4), the interesting formula

$$\mathbf{x}_0 = \mathbf{S}(\mathbf{S}^{\mathrm{T}}\mathbf{M}\mathbf{S})^{-1}\mathbf{S}^{\mathrm{T}}\mathbf{f}, \tag{C.9}$$

$$\sum_{m=1}^{\sigma} \boldsymbol{\Psi}_m \boldsymbol{\Psi}_m^{\mathrm{T}} = \mathbf{S}(\mathbf{S}^{\mathrm{T}}\mathbf{M}\mathbf{S})^{-1}\mathbf{S}^{\mathrm{T}}, \tag{C.10}$$

(b) Coefficient $\mathbf{X}_1$: Eq. (C.8) can now be carried into the second identification equation to deliver

$$\mathbf{K}\mathbf{x}_1 = \mathbf{f} - \mathbf{M}\mathbf{S}(\mathbf{S}^{\mathrm{T}}\mathbf{M}\mathbf{S})^{-1}\mathbf{S}^{\mathrm{T}}\mathbf{f}. \tag{C.11}$$

Singular linear systems of this type have been considered in Appendix B. The system is solvable since $\mathbf{S}^{\mathrm{T}}$ times the second member makes 0, which is not surprising because the second member results from the superposition of external loads with related inertial forces. According to the discussions of Appendix B, the solution can be determined only within an arbitrary rigid motion.

Because Laurent coefficients cannot suffer such an indetermination, subsidiary conditions have to be found elsewhere in the cascade (C.4), and more precisely in the third relation, which is the only other equation that contains $\mathbf{x}_1$. As a matter of fact, one can write

$$\mathbf{K}\mathbf{x}_2 - \mathbf{M}\mathbf{x}_1 = 0 \Rightarrow \mathbf{M}\mathbf{x}_1 \in \mathrm{Im}\mathbf{K} \Rightarrow \mathbf{S}^{\mathrm{T}}\mathbf{M}\mathbf{x}_1 = 0, \tag{C.12}$$

which are conditions of the type discussed in Appendix B. Eqs. (C.11) and (C.12) and the second projector theorem of Appendix B then bring

$$\mathbf{x}_1 = (\mathbf{1} - \boldsymbol{\Pi}_M)(\lambda\boldsymbol{\Pi} + \mathbf{K})^{-1}\left[\mathbf{1} - \mathbf{M}\mathbf{S}(\mathbf{S}^{\mathrm{T}}\mathbf{M}\mathbf{S})^{-1}\mathbf{S}^{\mathrm{T}}\right]\mathbf{f}. \tag{C.13}$$

Considering the expression (A.10) of $\boldsymbol{\Pi}_M$, one can now remark the complete symmetry between the left and right factors, and write

$$\mathbf{x}_1 = \left[\mathbf{1} - \mathbf{S}(\mathbf{S}^{\mathrm{T}}\mathbf{M}\mathbf{S})^{-1}\mathbf{S}^{\mathrm{T}}\mathbf{M}\right](\lambda\boldsymbol{\Pi} + \mathbf{K})^{-1} \left[\mathbf{1} - \mathbf{M}\mathbf{S}(\mathbf{S}^{\mathrm{T}}\mathbf{M}\mathbf{S})^{-1}\mathbf{S}^{\mathrm{T}}\right]\mathbf{f}. \tag{C.14}$$

or, more concisely,

$$\mathbf{x}_1 = (\mathbf{1} - \mathbf{\Pi}_M)(\lambda\mathbf{\Pi} + \mathbf{K})^{-1}(\mathbf{1} - \mathbf{\Pi}_M)^{\mathrm{T}}\mathbf{f}. \tag{C.15}$$

A very important relation can be obtained from a mere comparison with Eq. (C.3)

$$\sum_{m=\sigma+1}^{\overline{N}} \frac{\mathbf{\Psi}_m \mathbf{\Psi}_m^{\mathrm{T}}}{\omega_m^2}\mathbf{f} = (\mathbf{1} - \mathbf{\Pi}_M)(\lambda\mathbf{\Pi} + \mathbf{K})^{-1}(\mathbf{1} - \mathbf{\Pi}_M)^{\mathrm{T}}\mathbf{f}. \tag{C.16}$$

The coefficient $\mathbf{x}_1$, which coincides with the elastic displacement under external and inertial forces after "filtration" of rigid modes, corresponds to modern versions of what is generally called "the inertia relief" displacement or mode. The computation of such a displacement is a standard option in most finite element codes. Ancient versions, devoted to stress computation in uniformly accelerated vessels and not to modal synthesis however, replace the correct filtration of rigid modes by more simple, but inadequate, isostatic support conditions.

Formulae for higher-order coefficients can be derived in the same manner. For the sake of brevity, however, they will not be developed in the present study.

References

[1] M. Ghandchi Tehrani, W. Wang, C. Mares, J.E. Mottershead, The generalized Vincent circle in vibration suppression, *Journal of Sound and Vibration* 292 (2006) 661–675.

[2] M. Ghandchi Tehrani, W. Wang, C. Mares, J.E. Mottershead, Vibration suppression using Vincent's circle, *Proceeding of ISMA*, 2004, pp. 603–661.

[3] J.E. Mottershead, Structural modification for the assignment of zeros using measured receptances, *Journal of Applied Mechanics—Transactions of the American Society of Mechanical Engineers* 68 (5) (2001) 791–798.

[4] G.T.S. Done, A.D. Hughes, The response of a vibrating structure as a function of structural parameters, *Journal of Sound and Vibration* 38 (2) (1975) 255–266.

[5] O. Tanneau, O. Sauvage, J.M. Lagache, Analyse vibratoire de modifications de structures, L'approche des cercles de Vincent revisitée, *XVe Colloque Vibrations, Chocs et Bruits*, Ecole Centrale de Lyon, 14–16 juin 2006 (in French).

[6] A.H. Vincent, A note on the properties of the variation of structural response with respect to a single structural parameter when plotted in the complex plane, Westland Helicopters Ltd., Report GEN/DYN/RES/010R, September 1973.

[7] H. Schwerdtfeger, *Geometry of Complex Numbers–Circle Geometry, Moebius Transformation, Non-Euclidian Geometry*, Dover, New York, 1979.

[8] Z.–Q. Qu, Hybrid expansion method for frequency responses and their sensitivities, part I: undamped systems, *Journal of Sound and Vibration* 231 (1) (2000) 175–193.

[9] R. Ohayon, C. Soize, *Structural Acoustics and Vibration*, Academic Press, San Diego, 1998.

[10] R.R. Craig Jr., A review of time-domain and frequency-domain component-mode synthesis methods, *Journal of Modal Analysis* (1987).

[11] R.M. Hintz, Analytical Methods in Component Modal Synthesis, *AIAA Journal* 13 (8) (1975).

[12] D. Gottlieb, S. Gottlieb, Spectral methods for discontinuous problems, in: *Biennial Numerical Analysis Conference*, NA03, 2003, pp. 65–71 ⟨http://www.maths.dundee.ac.uk/~naconf/proc03/gottlieb.pdf⟩.

[13] D. Gottlieb, C.W. Shu, A general theory for the resolution of the Gibbs phenomenon. Accademia Nazionale Dei Lincey, *ATTI Dei Convegni Lincey* 147 (1998) 39–48.

[14] M. Tournour, N. Atalla, Pseudostatic corrections for the forced vibroacoustic response of a structure-cavity system, *Journal of Acoustical Society of America* 107 (2000) 2379–2386.

[15] M. Tournour, N. Atalla, O. Chiello, F. Sgard, Validation, performance, convergence and application of free interface component mode synthesis, *Computers & Structures* 79 (2001) 1861–1876.

[16] O. Sauvage, Modélisation du comportement vibratoire d'un groupe moto-propulseur de 0 à 10000 Hz, Thèse de doctorat, de l'Ecole Centrale de Paris, 2002 (in French).

[17] M. Geradin, D. Rixen, *Mechanical Vibrations: Theory and Applications to Structural Dynamics*, Wiley, New York, 1997.

[18] G. Strang, *Introduction to Applied Mathematics*, Cambridge Press, Welleslay, 1986.

[19] E. Balmès, *Use of Generalized Interface Degrees of Freedom in Component Mode Synthesis*, IMACs, New Brunswick, NJ, 1996, pp. 204–210.

[20] Y.Y. Kim, J.H. Kang, Inability of free-interface modes in representing stress resultants near the free interface, *Journal of Vibration and Acoustics* 122 (2000) 409–411.

[21] G.M.L. Gladwell, Branch mode analysis of vibrating systems, *Journal of Sound and Vibration* 1 (1964) 41–59.

[22] R.H. MacNeal, A hybrid method of component mode synthesis, *Computers & Structures* 1 (1971) 581–601.

[23] W.C. Hurty, Dynamic analysis of structural systems using component modes, *AIAA Journal* 3 (4) (1965) 678–685.

[24] R.R. Craig Jr., M.C. Bampton, Coupling of substructures for dynamic analyses, *AIAA Journal* 6 (7) (1968) 1313–1319.
[25] W.C. Hurty, J.D. Collins, G.C. Hart, Dynamic analysis of large structures by modal synthesis techniques, *Computers & Structures* 1 (1971) 535–563.
[26] S. Rubin, Improved component-mode representation for structural dynamic analysis, *AIAA Journal* 13 (8) (1975).
[27] W.A. Benfield, R.F. Hruda, Vibration analysis of structures by component mode substitution, *AIAA Journal* 9 (7) (1971) 1255–1261.
[28] R. Ohayon, R. Sampaio, C. Soize, Dynamic substructuring of damped structures using singular value decomposition, *Transactions of the ASME* 64 (1997) 292–298.
[29] E. Balmès, Optimal Ritz vectors for component mode synthesis using the singular value decomposition, *AIAA Journal* 34 (6) (1996).
[30] Ph. Destuynder, Remarks on dynamic substructuring, *European Journal of Mechanics A—Solids* 8 (3) (1989) 201–218.
[31] F. Bourquin, F. d'Hennezel, Numerical study of an intrinsic component mode synthesis method, *Computer Methods in Applied Mechanics and Engineering* 97 (1992) 49–76.
[32] J.N. Reddy, *Applied Functional Analysis and Variational Methods in Engineering*, McGraw-Hill, New York, 1986, pp. 229–231.
[33] J.L. de Lagrange, *Méchanique analitique*, Paris, 1788 (reprinted by J. Gabay Ed., Paris, 1989, pp. 44–49).